ABSTRACT

YANG, CHIH-HSIANG. Nano-Crystalline Manipulation to Achieve Laser-based Crack-Free Edge Isolation for Silicon-Based Solar Cells. (Under the direction of Dr. Juei-Feng Tu).

Using silicon-based solar cells with high efficiency and long lifespan as a renewable and green energy source can not only greatly reduce dollar-per-watt ratios but also be eco-friendly. During the manufacturing of solar cell, a very important step called edge isolation process affects IV characteristics of solar cell, which is critical to the efficiency of itself. Deep and crack-free edge isolation to increase shunt resistance in the solar cell achieves higher efficiency and eliminates the source of fatigue cracks to extend lifespan of solar cells. The deeper edge isolation grooves can be created by focusing the laser deep into the solar cell substrate. However, previous experiments done on Si wafer using pulsed laser shows there is possibility of void generation when laser is focused deep into the material. In addition, compared with shorter wavelength (532 or 355nm), the laser absorption of silicon wafer is less and the possibility to form micro cracks is higher during the processing of fiber laser with 1064-nm wavelength. Silicon wafers are semi-transparent to the near infrared light and have a temperature dependence of optical property that a higher temperature leads to higher laser energy absorption. By manipulating temperature of solar cells combining with scribing speed, focus position, and laser power of solar cells, it is confirmed from the experiments that deeper and narrower grooves can be scribed using Continuous Wave (CW) laser to maximize the active area of solar cell and consequently, its efficiency. The depth of the grooves can be initially predicted from the 2D model for different speeds and powers. The experiments are conducted by using 300W single mode fiber laser with 1075-nm wavelength.

Nano-Crystalline Manipulation to Achieve Laser-based Crack-Free Edge Isolation for Silicon-Based Solar Cells

by
Chih-Hsiang Yang

A thesis submitted to the Graduate Faculty of
North Carolina State University
in partial fulfillment of the
requirements for the degree of
Master of Science

Mechanical Engineering

Raleigh, North Carolina

2012

APPROVED BY:

_____	_____
Dr. Fuh-Gwo Yuan	Dr. Chih-Hao Chang

_____

Dr. Juei-Feng Tu

Chair of Advisory Committee

BIOGRAPHY

Chih-Hsiang Yang was born September 12th, 1984 in Taichung, Taiwan. When he was young, he had strong interest in assembling robotic and car toy model, and that was how he developed his aspiration to become an engineer. Chih-Hsiang then attended National Chiao Tung University (NCTU), notably top 3 of the finest institutions in Taiwan, studying mechanical engineering as an undergraduate. After graduating in the spring of 2007 from NCTU with a Bachelors of Science in Mechanical Engineering, and decided to pursue an advanced degree in mechanical engineering in the U.S., in order to have not only the advanced knowledge in mechanical engineering but also wider international vision. Having carefully reviewed the various options he had, he decided to pursue his degree at the North Carolina State University. In his first semester of master studies at North Carolina State University he had the privilege of meeting Dr. Juei F. Tu from which this current research relationship stemmed. He will receive his Master of Mechanical Engineering degree in December 2012 with a concentration in laser manufacturing processing.

ACKNOWLEDGMENTS

First of all, I would like to thank Dr. Juei-Feng Tu, for his guidance during my master study. He is not only a good advisor in academic part but also a thoughtful tutor in my life journey, providing me good hints and assistances while I encountered problems in my research and different points of view to philosophy in terms of life and society. He does inspire me a lot. Also, I would also like to acknowledged Dr. Fuh-Gwo Yuan and Dr. Chih-Hao Chang for serving on my committee. Finally, Nilesh Rajule, my senior labmate, thank him for teaching me the operations of all the equipments and software in our laboratory and the way to write this thesis; Nicholas Reeves, the other labmate, also helped me a lot, and we often encouraged each other to move forward. I cannot finish this thesis without those people, and I am truly grateful for all your help.

TABLE OF CONTENTS

LIST OF TABLES

LIST OF FIGURES

1. INTRODUCTION

Solar energy, radiant light and heat from the sun, is a clean, reliable, and renewable source of power. Among all the renewable energy sources such as wind, tides, and geothermal energy, solar power is the primary source of energy. We humans have always harnessed the energy of the sun as far back as we have existed on the planet using a range of ever-evolving technologies; without it, life would not exist on our planet.

Nowadays, although there are many renewable source of power, humans still rely on the conventional energy resource, and fossil fuels are the main sources that we use every day. As far as convenience and efficiency are concerned, consumption of fossil fuels can be seen everywhere in our daily life, from generation of electricity to power source to drive vehicles. However, this kind of resources is not infinite. In addition, they cause the main air pollution which is attributed to the global warming when burned. Compared to fossil fuels, the sun is unique and infinite source of free and clean power, delivering more than 1000 kWh/m^2, and this amount is equal to 100 liters of heating oil. It would be great if the solar energy can be used more widely and more efficiently.

Another source of energy secondary to fossil fuels is nuclear power, which is considered to mitigate global warming. Nuclear power generation have many advantages, such as relatively low emission of carbon dioxide and high density of electricity generation, nevertheless, there are lots of severe disadvantages of it. The radioactive waste from nuclear energy is dangerous and cannot be disposed safely. Moreover, building a nuclear plant with 100% security is impossible; the consequence of martial attacks, natural disasters or accidents like Japan nuclear crisis caused by earthquake would be absolutely devastating not only for human being but also the nature. For several reasons, nuclear power is neither green and sustainable nor renewable.

Unlike fossil fuels and nuclear power, which are harmful to the earth, renewable energy has less impact on the environment. Although renewable energy production has some drawbacks, mainly associated with the use of large of tracts of land that affects animal habitats and outdoor scenery, the clean, sustainable, and reliable properties of it are still appealing.

Solar power, which can be converted into electricity by solar cells, is the primary source of power among all the renewable energy sources. Solar cells are made of silicon around 95 percents and are also are described as photovoltaic cells when the light source is not necessarily sunlight (lamplight, artificial light, etc.). Crystalline-silicon and thin films are the two widely used form of solar cells. The awareness of using solar cell technology to produce energy has been increasing; nowadays, the electricity generated through solar technology is widely being used to power homes, cars and appliances. This has made solar technology to be one of the most important advances in technology in recent times.

2. BACKGROUND INFORMATION

2.1 Si-based Solar Cell

Solar cell, which is usually made of crystalline silicon, is an electrical device that can convert the energy of the light into electricity. Since the si-based solar cell is a semiconductor material that has special electrical properties, it allows the emission of electrons when light shines on the surface of the material, known as photovoltaic effect(PV effect). After that, electrons flow out of the solar cell, and a current is formed. (Scott 2000)

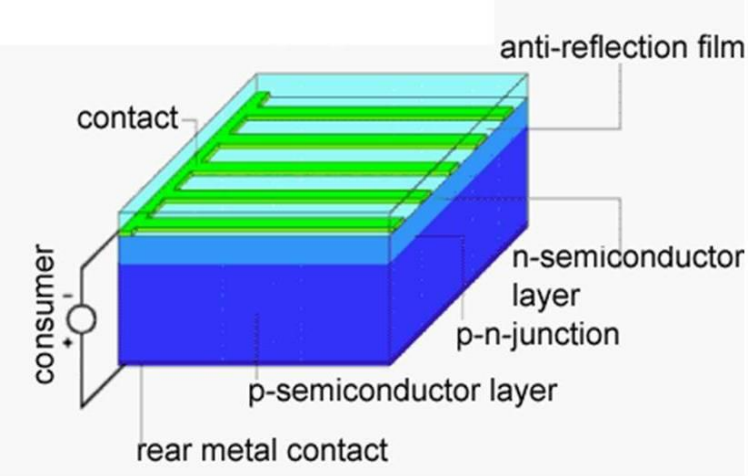

Figure 2.1 Model of a crystalline solar cell (Solar Energy Ireland 2000)

A Silicon-based solar cell consists of several different parts, as shown in Figure 2.1. How silicon makes a solar cell and how it converts light directly into electricity? First of all it starts with highly purified silicon. From the periodic table, it is known that a silicon atom totally has fourteen electrons, and the outer shell, however, is only half full with just four electrons. In order to stay in the stable state, a silicon atom will share electrons with four nearby atoms; each atom has four hands joined to four neighbors. That's what forms the crystalline structure. (ibid)

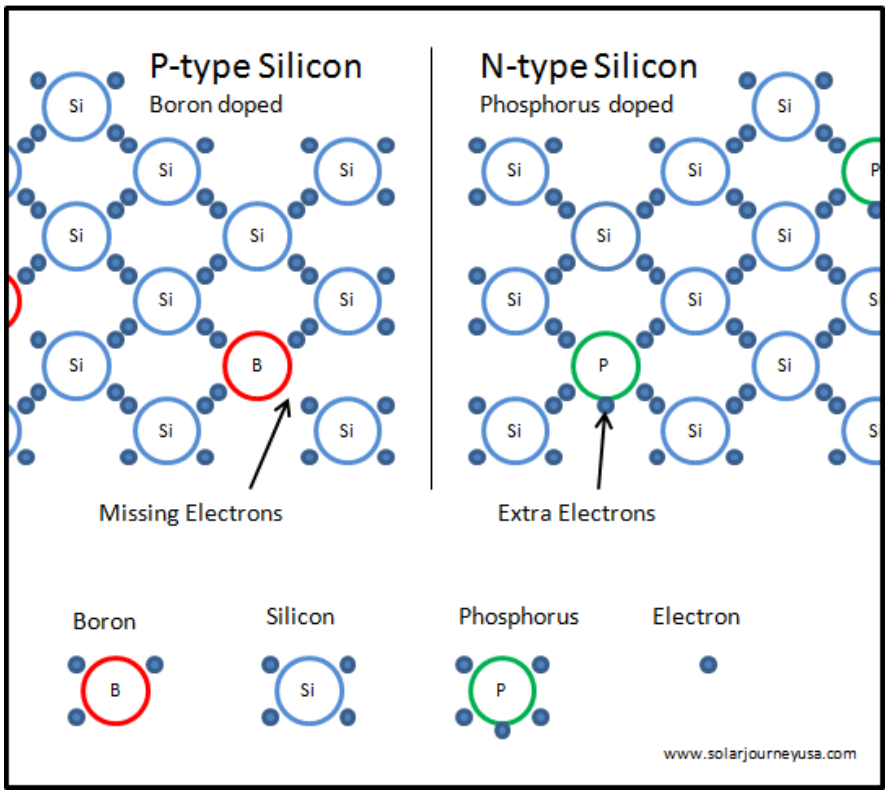

Figure 2.2 P-type and N-type Silicon Semiconductor(Solar Journey USA)

Since the electrons are unable to move freely in the crystalline structure due to the strong bonds between each atom, pure crystalline silicon is a poor conductor of electricity. A process called doping, which means adding impurities to the pure silicon, can improve its conductivity. As shown in Figure 2.2, boron, which only has three electrons in the outer shell, is doped into the silicon to form a free "hole"(missing electron). This kind of doped silicon is called p-type silicon because one electron is missing, and it has free openings and carries the positive charge. On the other hand, phosphorous has five electrons in its outer shell, so it creates additional free electron when combing with silicon. Silicon doped with phosphorous is called n-type because of the prevalence of free electrons, relatively negative. (ibid)

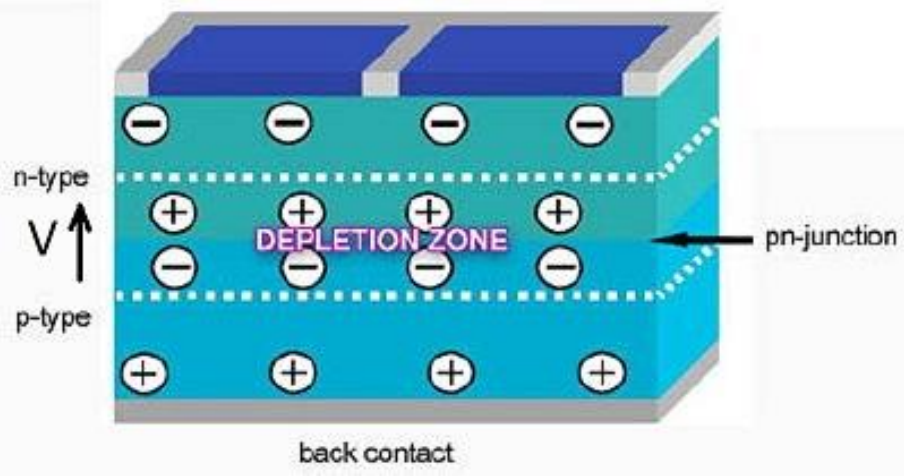

Figure 2.3 P-N Junction and Depletion Zone (SPECMAT Ltd. 2009)

When the silicon wafers respectively are doped with boron(p-type) and phosphorous(n-type), they are electrically neutral. However, if the p-type and n-type silicon come into contact, P-N junction is formed. The electrons diffusing across the junction from n-type side into p-type side quickly recombine with some of the majority holes there, likewise holes moving from the p-type side to the n-type side, then forming electron-hole pairs. Figure 2.3 illustrates the diffusion. After the equilibrium of diffusion of electrons and holes is reached, a "barrier" called depletion zone shown in Figure 2.3 appears, resisting the further transfer which makes it more difficult for electrons to move from n-type side into p-type side. Therefore, an electric field separates the two sides. (ibid)

As light, in the form of photons, with enough energy, are incident on the solar cell, electron-hole pairs are broken by them, each of them freeing exactly one electron. The electric field will send the electron to the n-side and the hole to the p-side. When an external current path is provided, like the consumer in Figure 2.1, electrons will flow through the path to the p-type side to unite with holes that the electric field sent there; a current is formed. In addition, the cell's electric field provides a voltage. With both current and voltage, the power is generated. (ibid)

2.2 I-V Characteristic of Solar Cell

In principle, a solar cell is a simple semiconductor device that converts light into electric energy, also called PV (Photovoltaic) cells. The conversion is accomplished by absorbing light, then ionizing crystal atoms creating free, negatively charged electrons and positively charged ions, and that is how current is formed. In addition, the p-n junction forms electric field providing voltage output. Therefore, one can use solar cells as a power source.

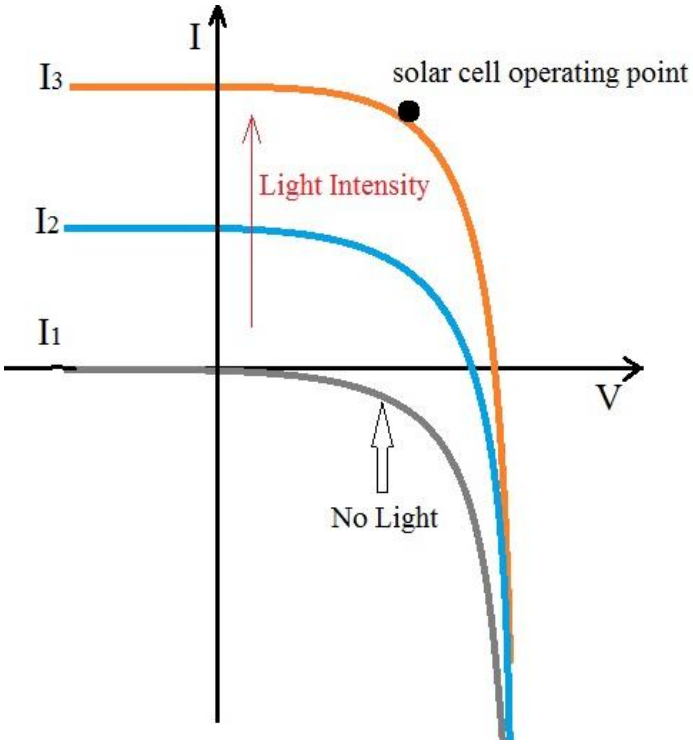

Figure 2.4 IV curve for solar cell and solar cell as current source parallel with diode

The performance of solar cell is determined by estimating the generated power output. The solar cell has current-voltage characteristic curves representing the relationship between current and voltage produced by the solar cell, which are nonlinear and rectifying as shown in Figure2.4. I-V curves are plotted in a condition that the exposure of light is maintained at constant level at constant cell temperature.

In Figure 2.4, the x-axis and y-axis represent the voltage and current, respectively. It shows that the I-V curve will lift up when the intensity of incident light increases, but it is still the same as the curve in diode mode. The solar cell is usually operated in reverse bias mode. Solar cell acts as a diode when there is no current produced without light incident to it. Depending on both the intensity and wavelength of the incident light, solar cell can produce different current, which is proportional to the intensity of incident light. (National Instruments, 2009)

Let I_l be the current produced by the photoelectric effect and I_D be the diode current in an ideal cell. The total current I is calculated from the difference between I_l and I_D.
The equation (ibid) for the total current I is written as,

$$I = I_l - I_D = I_l - I_0(e^{qV/kT} - 1) \quad (2.1)$$

Where I_0 – Saturation current of the diode

q – Elementary charge $1.6x10^{-19}$ Coulombs

k – Constant of value $1.38x10^{-23}$J/K

T –Cell temperature in Kelvin

V–Measured cell voltage which is either produced or applied

The above equation (ibid) can be expanded to,

$$I = I_l - I_0(\exp^{[q(V+I.Rs)/n.k.T]} -1) - (V+I.R_s)/R_{sh} \quad (2.2)$$

Where R_s – Series resistance

R_{sh} – Shunt resistance

n- Diode ideality factor. It is the measure of how closely a diode follows the ideal diode equation. Its value is between 1 and 2.

The equivalent circuit of the solar cell is shown in Figure 2.5.

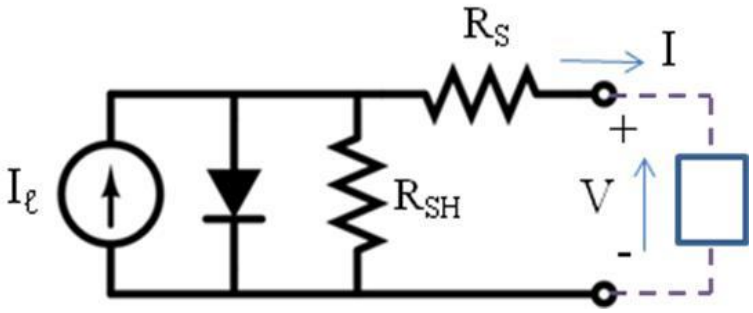

Figure 2.5 Equivalent circuit for the solar cell (National Instruments, 2009)

The load resistance is varied from zero to infinity and the I-V graph is plotted. I-V curve is shown in Figure 2.6. I_{SC} represents the short circuit current and V_{OC} represents the open circuit voltage.

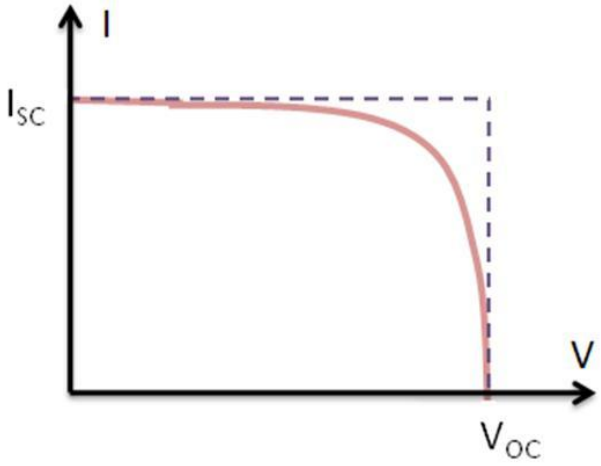

Figure 2.6 IV curve for Solar cell (National Instruments, 2009)

2.2.1 Fill Factor (FF)

Fill Factor is measured as the rectangular area of I-V curve. It is the measurement of quality of a solar cell. The Fill Factor can be calculated by comparing maximum power (P_{MAX}) to the theoretical power (P_T). Theoretical power can be assumed as power output at short circuit current and open circuit voltage. (ibid)

$$FF = P_{MAX} / P_T = (I_{MP}.V_{MP}) / (I_{SC}.V_{OC}) \quad (2.3)$$

Where $I_{SC} = I_{MAX} = I_l$ for forward bias quadrant

$V_{OC} = V_{MAX}$ for forward bias quadrant

I_{MP} and V_{MP} = current and voltage at the maximum power point, respectively

The Fill Factor represents the degree to which the voltage at the maximum power point matches with the open circuit voltage and to which the current at the maximum power point matches with the short circuit current. (ibid)

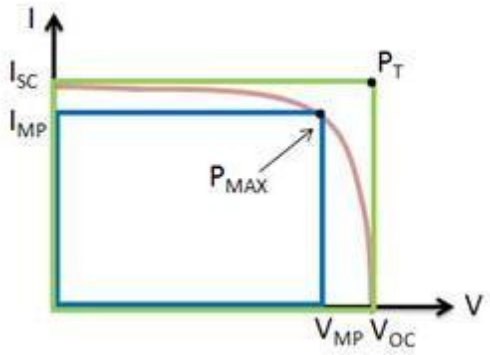

Figure 2.7 Fill Factor (National Instruments, 2009)

The larger fill factor is desired as it approaches to the rectangular area of IV curve. Fill Factor is represented in percentage. Typically values of fill factors are between 0.5 and 0.82. The efficiency of the cell is decreased due to the loss of power across internal resistances. These resistances are represented as shunt resistances and series resistances in the equivalent circuit diagram of the solar cell. In an ideal situation, it is desired that the value of shunt resistance is infinite and the series resistance should have zero value. If the shunt resistance has infinite value, it will not provide an alternate path for current and if the series resistance has zero value, there will not be any voltage drop before the load. (ibid)

2.2.2 Shunt Resistance (R_{SH}) and Series resistance (R_S)

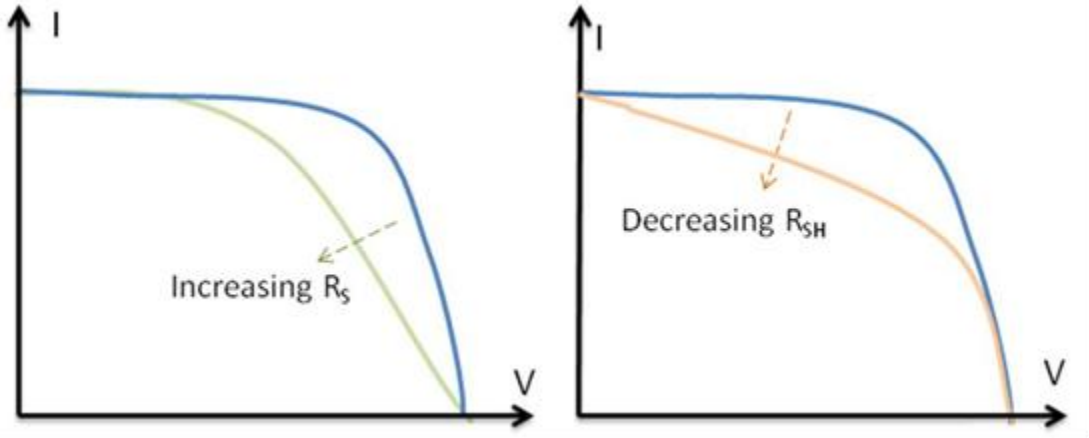

Figure 2.8 Effect of series and shunt resistances on IV curve (National Instruments, 2009)

Figure 2.8 shows the effect of resistances on the IV curve. Increasing the series resistance and decreasing shunt resistance will decrease the fill factor hence will decrease the efficiency of the solar cell. To achieve the maximum efficiency, the value of shunt resistance should tend to infinity and the value of the series resistance should tend to zero. Though infinite shunt resistance is desired for maximum power output of the solar cell, during the manufacturing process of the solar cell, an alternate conducting path is formed between p-type and n-type semiconductor layers resulting in decreased shunt resistances. (ibid)

2.3 Manufacturing of Si-based Solar Cell

Nowadays, the manufacturing of silicon-based solar cell is relatively energy-intensive process which involves polishing, etching, and doping of silicon wafer. Since silicon wafer fabrication and solar cell module assembly accounts for 25 to 30 percent of the total cost, many plants are built at a site where there is an abundant source of reliable and cheap energy to reduce the cost of manufacturing process. Furthermore, many solar cell plants are located near crystal growing and casting plants to secure a wafer supply to their cell plants, which means they are a very close chain, cannot be separated. (How Products Are Made)

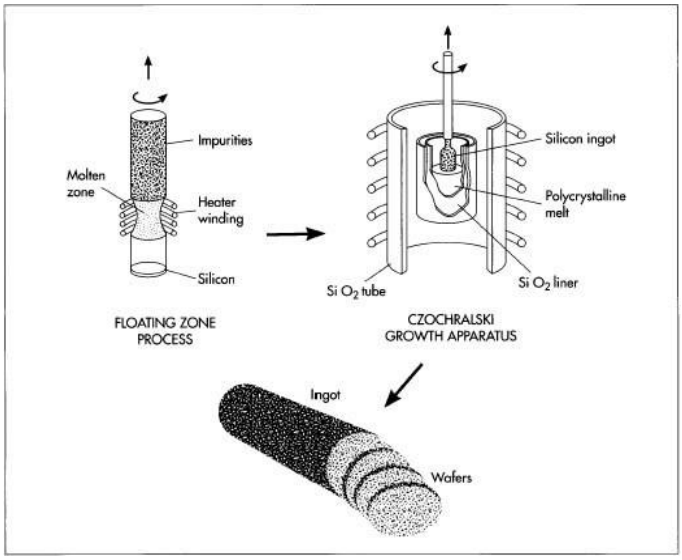

Figure 2.9 Principle of Different Silicon Wafer Manufacturing Processes (How Products Are Made, 2006)

2.3.1 Purifying Silicon

Silicon, the raw material of solar cell, is the second most abundant element available on earth; It usually exists as a form of silicon dioxide like sand or crushed quartz. Silicon is derived from silicon dioxide in an electric arc furnace, where a carbon arc is applied to release the oxygen. The products are carbon dioxide and molten silicon; however, the resulting silicon with 99 percent of purity is still not good enough to be processed for solar cells, requiring further purification.

After the initial purification, the 99 percent pure silicon can be purified even further in the floating zone process shown in Figure 2.8 to reach the standard of solar cell industry. To eliminate the one percent impurities, a rod of silicon is passed through a heated zone several times in the same direction. Consequently, the impurities are dragged toward one end with each pass, then removing the impure end; the rest of silicon is considered pure.

2.3.2 Making Single Crystalline Silicon

Solar cells are made from silicon wafer sliced from silicon ingot, and single crystalline silicon is preferred for fabrication of solar cell. A process called Czochralski method shown in Figure 2.8 is developed to make single crystalline silicon from polycrystalline structures. In this process, a seed crystal of silicon is dipped into melted polycrystalline silicon. When the seed crystal rotates as it is withdrawn, a cylindrical ingot of silicon is formed. Pulling speed of seed crystal is adjusted depending on the desired size of silicon wafer, and meanwhile, the temperature of molten silicon is maintained.

2.3.3 Producing silicon wafers

Silicon wafers for solar cell manufacturing, whose thickness is around 200 to 300 microns, are sliced from the silicon ingot using single-thin metal saw coated with diamond. Since the silicon is a fragile material, during the slicing process, one-half of the silicon is wasted in the form of sawdust, produced from each cut as wide as the diamond saw. In addition, more material is most if the wafer is cut into rectangular or hexagonal shape. Silicon wafers in rectangular or hexagonal shape is good for solar cell assembly in terms of space; they can be fitted together perfectly.

2.3.4 Wafer Polishing and Etching

To have good electrical and optical properties, silicon wafers for solar cell need extra processing. The solar cell surface becomes glassy after polishing by using chemicals, and mirror-like surface provides good junctions with metals for electrical contacts. On the other hand, however, the surface is not good for light absorption, so pyramid texture needs to be added to it, done by chemical etching after the metal contacts are made. After that, the surfaces of silicon wafer are improved to be good absorption of light as it provides oblique surface to the incident light.

2.3.5 Doping and P-N Junction

To dope silicon wafer, a small amount of boron is introduced to it during Czochralski process so that it becomes p-type silicon. The wafer is then heated to the melting point of silicon in a furnace with phosphorous gas. To ensure a uniform p-n junction of proper depth, the top few microns of the wafer is converted to n-type, and the temperature and time given to the process is carefully controlled.

2.3.6 Placing front electrical contacts and back metal coating

Electrical contacts provide connection to each solar cell to another and to the receiver of produced current. The contacts in the front, which are made of silver, nickel or copper, have to be very thin to ensure more available surface area for incident light. On the other hand, the back metal coating is for reflecting back the light which penetrates though the wafer to increase the efficiency of solar cell.

2.3.7 Applying Anti-Reflective Coating

To reduce the amount of light lost up to 35 percent due to the shiny surface of silicon, the transparent anti-reflective coating is applied on the top surface of solar cell to have maximum absorption of incident light. The material of anti-reflective coating most commonly used is silicon oxide. There are two ways to do it, either sputtering the material or make the silicon wafer itself to react with oxygen- or nitrogen-containing gases to form silicon oxide or nitride with thickness less than 0.1 micron.

2.3.8 Edge Isolation

The main purpose of edge isolation is to isolate p-type and n-type silicon electrically. Without proper edge isolation, an undesirable electric path will form to allow electrons liberated by sunlight to rejoin positive carriers (the holes) instead of flowing through the external circuit. This topic will be further discussed in detail in 2.5.

2.4 Quality and Efficiency of Si-based Solar Cell

In solar cell manufacturing, quality is considered one of the most important things since the overall efficiency of the solar cell can be greatly or adversely affected by the differences in the manufacturing processes. Many researchers are concentrating on improving the efficiency of each solar cell over a longer lifetime and finding a new process to replace the conventional one. The efficiency of solar cells being used these days is between 14 and 18 Percent. (Markvart & Castaner, 2005)

Efficiency of the solar cell is defined as the percentage of incident light absorbed by solar cell then converted into electricity. It is the ratio of output power of the solar cell to the input power of the incident light.

$$\eta = P_{out} / P_{in} \quad (2.1)$$

At the maximum power point, the solar cell operates at maximum efficiency.

$$\eta_{MAX} = P_{MAX} / P_{in} \quad (2.2)$$

The way to calculate the input power converted from incident light is the product of the light irradiance and the surface area of solar cell. Except for the intensity and wavelength of the light, there are other factors like natural resistance, temperature, reflection and electric resistance which affect the efficiency of the solar cell.

2.4.1 Improving efficiency

There are several ways to improve efficiency of solar cell. First of all, the efficiency can be improved by changing the design of solar cell. When higher efficiencies are desired, adding a semiconductor of lower gap on the bottom as tandem solar cells can be beneficial. In this case, the photons not absorbed in the top cell can be absorbed at the second layer. (Gee and Virshup, 1988) Furthermore, different materials with better light absorptivity such as mono-crystalline photovoltaic or conductive polymers can convert light into electricity more efficiently. (National Instrument, 2009)

Although the efficiency of solar cell can be increased by using different materials or design, the improvement is limited and the manufacturing cost is still high. Most current research therefore aims for increasing this efficiency or reducing solar cell cost in order to have higher price/performance ratio solar cell. There are innovations needed to replace the conventional manufacturing methods or to develop cheaper alternatives to expensive solar cell.

2.4.2 Solar Cells with Shunts

The shunt is an undesired path with lower resistances for current flow, causing efficiency loss due to the emitter at the edge of the cells or the metal contacts. Shunted cells significantly reduce average efficiencies, result in modules with poor low light performance and reduce the total yield. (Abbott, 2007) In solar cell, as the current generated by photons leaks though the shunts it decreases the current generated by solar cell thereby reducing the fill factor and the open circuit voltage. (Breitenstein,2004)

Shunt cans be defined as any local site where the local current exceeds the homogeneously flowing current. There are several types of shunt have been found in mono- and multi-crystalline solar cells. These shunts are different by the type of their I-V characteristics (linear or nonlinear) and by their physical origin. In general, shunt types can be either process-induced or caused by grown-in defects of the material. The most dominant type of shunt is linear edge shunt, which is process-induced, due to incompletely opened emitter at edge. The incompletely opened emitter is caused by improper edge isolation techniques, which is to isolate n-type layer and p-type cell electrically. (Breitenstein,2004)These shunts are accounted for 80% of the loss of power. The electrical isolation between p-type and n-type semiconductors can be achieved by creating a groove along the edges. (Hamammu and Ibrahim, 2002)

Another type of process-induced liner shunt occurs because of the cracks in the silicon wafers, so-called volume shunts, as shown in Figure 2.9. Volume shunts are caused by material defects in the bulk. Volume shunts are accounted for 20% of the loss occurs due to shunts After the process of doping the n-type layer, it is possible that during adding the front metal contact or back metal coating, metal paste penetrates through the cracks, providing conduction between the p-n junction. (Breitenstein,2004) These shunts cannot be removed without destroying the solar cell; however, shunted regions isolation technique can reduce the impact of shunted regions in poor quality solar cells. The technique can increase the efficiency of a badly shunted solar cell from 9.6% to 13.3%. (Abbott, 2007)

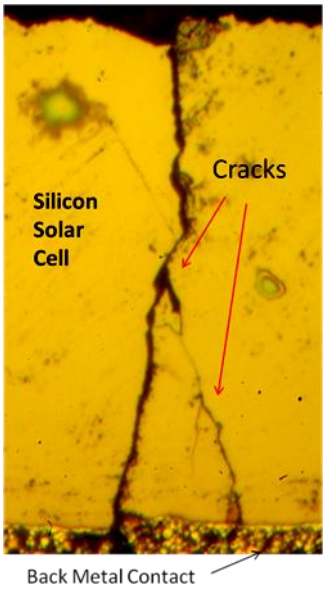

Figure 2.10 A commercial solar cell with a fatigue crack through the whole cell.

2.5 Edge Isolation

Edge isolation is a very important part of all silicon-based solar cell production process, and it greatly affects the efficiency of the cells. The main purpose of edge isolation is to isolate p-type and n-type silicon electrically. Without proper edge isolation, an undesirable electric path (shunt) will form to allow electrons liberated by sunlight to rejoin positive carriers (the holes) instead of flowing through the external circuit. The edge isolation process is to remove the phosphorous diffusion (n-type layer) with a thickness 10 to 20 µm around the edge of the cell by creating narrow and continuous grooves through the boron diffusion (p-type layer) so that the front emitter is electrically isolated from the cell rear, as shown in Figure.2.9. To optimize the isolation grooves to ensure the maximum area for sunlight absorption, those groove must be as close as possible to the edges of the front surface and as narrow as possible.

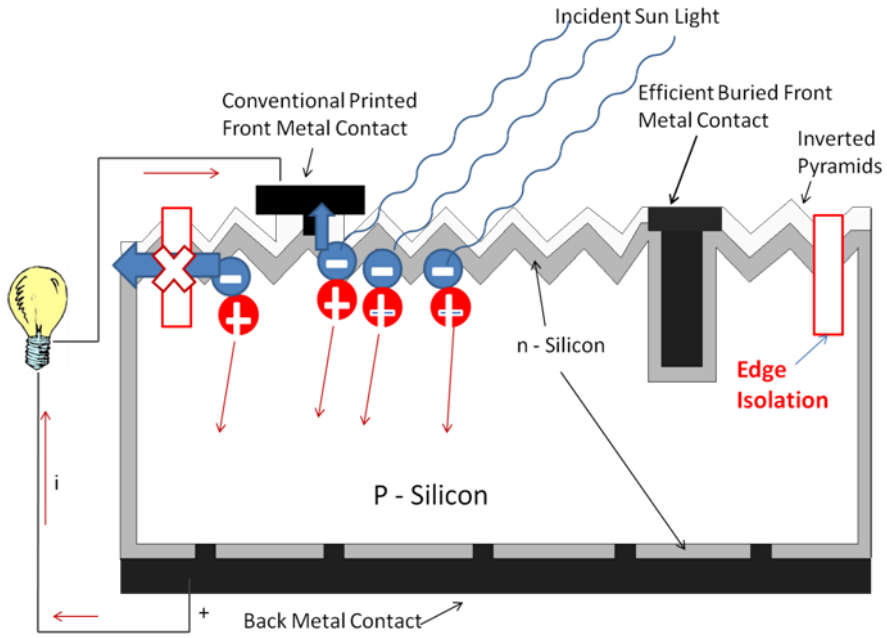

Figure 2.11 A functional Si-based solar cell panel with metal contacts and anti-reflection coating

By creating isolation grooves to isolate p-type and n-type silicon electrically, the edge shunt can be removed. Many different techniques to achieve edge isolation have been developed, including laser isolation, mechanical edge isolation, plasma edge isolation, and wet chemical etching.

3. LITERATURE REVIEW

3.1 Laser Edge Isolation

The laser edge isolation of solar cells is a new mechanical process to melt and evaporate material by scribing the cells with laser beam to remove edge shunts pathway. A laser-scribed thin groove through the n-type to p-type layer along the edges can make the front emitter electrically isolated. Typically, groove is 10 to 20 μm deep and less than 20 μm wide.

In most solar cell processes, edge isolation is an important step. To reduce the dominant cost within silicon-based solar cell manufacturing, wafers with larger size thinner than today's industry standard of 220 μm are considered dominant in the next generation. Since thinner and larger wafers are increasingly fragile and mechanically vulnerable, needless to say, the noncontact nature of laser edge isolation processes offers profound benefits versus any contact-based alternative. In addition, the laser processing is fast, easy to align and no chemicals or susceptible mechanics are needed compared to wet chemical etching and plasma edge isolation. The greener processing is one of the clear advantages of laser that can resonate with solar company mission statements and marketing campaigns. (Colville and Dunsky, 2008)

However, the laser technique is not perfect. Lower laser intensity leads to insufficient depth of the isolation grooves, resulting in lower shunt resistance that can damage the efficiency. On the other hand, there is a possibility that micro cracks can be formed during laser processing with 1064 nm wavelengths or when the grooves are too deep. Any micro crack can become crack fronts, leading to crack propagation and eventual total fractures and cell failure. In addition, internal shunts can be formed when micro cracks combing with metal paste during the metal contact coating. Micro cracks are the key limit factor since they greatly decrease the yield of production lines. There are needs to eliminate those disadvantages to make the laser processing better. (ibid)

3.2 Plasma Etching Edge Isolation

Plasma etching of wafer stacks to remove shunts is a very common technique in industry and has been the standard procedure for silicon-based solar cell for many years. In the process, the solar cells are stacked together and then are put into a vacuum chamber. The etching is done in a fluoride/oxide plasma environment. The waste gases produced by plasma etching are toxic and need to be filtered and washed before disposal into atmosphere. Typically material of thickness 2-5 μm is removed from the edges as the front n-doped area is electrically isolated from the back contact surface. (Arumughan, *et al*, 2005)

The reasons why plasma edge isolation is so common in industry are because the coin stacking method ensures high throughput and low cost per wafer. This method also avoids handling of dangerous chemicals, produces less waste of silicon and ensures larger active area of solar cell. The waste silicon mass produced when processing 500 wafers sized $125 \times 125 mm^2$ is less than 9g. However, this method is not in-line process; as the stacking of the wafers is required, careful handling of the wafers is required for stacking and reducing the wafer damages. Since the next-generation solar cell will be thinner and larger in order to potentially reduce the process cost, alternative methods need to be developed to replace the plasma etching edge isolation due to non-in line process and mechanically vulnerable property of silicon wafers. (ibid)

3.3 Wet chemical Etching Edge Isolation

In chemical etching process, the edge isolation is done chemically by removing the rear side emitter after the light emitter diffusion. The wafers travel through an etching bath which is filled up to a certain level to achieve that only one side of the wafers in is contact with the etching solution. The etching parameters (etching depth and speed) can be varied depending on the wafer transport velocity, etching bath concentration and temperature. There is no loss in active cell area because this technique removes only 5 μm from the rear side. The waste silicon mass produced when processing 500 wafers sized 125×125mm² is 91g (Arumughan, *et al*, 2005)

Compared to laser isolation, the process involves stacking of the wafers as plasma etching, so careful handling of the wafers is required for stacking and reducing the wafer damages. There is a new method is developed by RENA with InOxSide tool. This is in-line process hence the continuous production line is not interrupted. The main advantage of this process is that the front side of the wafer is not damaged as it does not come in contact with the etching chemical. Nevertheless, the most important thing is, the etching of the edges is carried out by the chemicals like KOH, which is hazardous to human body and the environment. Using solar cell is a concept that is eco-friendly and is considered as a green energy, so there is no point to involve toxic chemical that is harmful to the nature during the manufacturing process.

3.4 Conventional Mechanical Edge Isolation

Conventional mechanical edge isolations include grinding the wafer edge with sandpaper, cutting the edge with a diamond dicing saw, and sawing grooves with a diamond dicing saw. Typically, thickness of the dicing saw is 0.1 μm. During the edge isolation process, material of thickness 1-2 mm is cut or grinded from the edges. After the edge isolation process, the active cell area is reduced by 3-6%, resulting in reduction of the short circuit current produced by the cell.

Although those conventional methods can provide good shunt resistance, so they have better performance in terms of efficiency, a huge amount of silicon debris are generated during the process; this waste cannot be recycled. The waste silicon mass produced when processing 500 wafers sized 125×125mm² is 174.75g. Moreover, compared to other methods, conventional mechanical edge isolation results in a loss of active area. Due to the brittle nature of silicon-based solar cell, the contact nature of grinding or cutting methods potentially damages the solar cells, leading to crack propagation and eventually total fractures.

We can summerize the different edge isolation techiniques in the following table.

Table 3.1Comparison of different edge isolation techniques (RAJULE, 2009)

Edge Isolation Process	**Process Technique**	**Production Technique**	**Disadvantages**
Mechanical	Cutting off edges	In-Line	Waste of material
Chemical/Plasma Etching	Etching away n-type layer from sides	Stacking of wafer	Hazardous Environment
Laser	Scribing along the edges	In-line	Higher power induces cracks

4. RESEARCH OBJECTIVE

The research objectives of this thesis are to

- To investigate the feasibility of temperature manipulation for crack-free laser isolation
- To investigate the effect of laser focusing, power and speed on the depth and width of the edge isolation groove.
- To optimize the systematic process design for crack-free isolation with sufficient groove width and depth

With respect to above research objectives, the following research approaches are conducted:

- Study of temperature dependent optical properties of silicon
- Modeling the laser scribing process
- Experimental investigation for the effects of temperature control, laser focusing, power and scribing speed.
- Optimize the process design to select temperature,laser focusing, power and speed systematically.

5 RESEARCH APPROACHES

To reach those research objectives mentioned above, we will first investigate temperature dependent optical properties of crystalline silicon under intensive laser irradiation. This investigation is conducted via literature review and experimental validation proposed by Ohmura et al, 2008. The absorption of laser energy by silicon is strongly influenced by its temperature; in general, a higher temperature leads to a higher absorption . Taking advantage of this property, we intend to create two phenomena for silicon processing purposes. The first phenomenon is called Avalanche Absorption and the second one is called Guided Thermal Shock.

5.1 Avalanche Absorption and Guided Thermal Shock

The avalanche absorption can be induced because a laser beam can liberate more free carriers along its optical path. The liberated carriers in turn enhance laser absorption, leading to more liberated carriers. The interaction between the laser and the doped silicon, therefore, is a closed-loop process. In some extreme cases, the absorption becomes unstable, leading to the avalanche absorption at a localized spot. When the avalanche absorption occurs, the localized avalanche spot becomes completely opaque to the laser beam to absorb all the laser energy. This localized energy absorption induces a sharp temperature gradient and high thermal stress, forming a thermal shock propagating away from the avalanche spot. Because silicon is semi-transparent to the near infrared wavelength, we can focus a high quality laser beam, such the one from a single mode fiber laser, inside the silicon to create such an avalanche spot.

Thermal shock is phenomenon which occurs usually in brittle materials when they are subjected to rapid and extreme temperature fluctuations, leading to uneven expansion. This uneven expansion causes expansion of molecular to induce stress on the molecular structure of the material. If the thermal gradient is high, this expansion of molecular bond overcomes strength of material, causing the crack front to advance. The main factors causing thermal shock are low toughness, low thermal conductivity and high thermal expansion coefficient of the material. Interestingly, the induced thermal shock can be "guided" so that it does not propagate in all directions. (Thermal Shock – Wikipedia)

5.2 Temperature Dependent Optical Properties of Crystalline Silicon

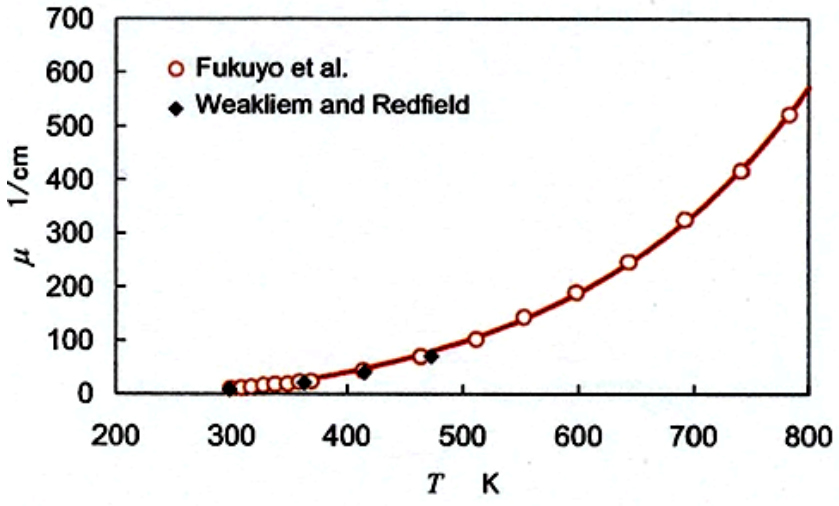

Figure 5.1 Measurement of laser absorption coefficient versus temperature up to 800K(Ohmura et al, 2008)

The absorption of laser energy by silicon is strongly influenced by its temperature; the absorption coefficient μ increases at elevated temperatures due to temperature dependent optical properties of crystalline silicon. The laser absorption coefficient of silicon as a function of temperature is shown in Figure 5.1. The relationship reported is on up to 800 K. According to Figure 5.1, the absorption coefficient at 400 K is 40 1/cm and becomes 560 1/cm at 800 K, which is 14 times the value of 400K. To put these values into perspective, an incident laser beam after advancing 10 μm inside a silicon wafer at 400 K will lose 4% of its intensity, absorbed by the silicon; while at 800 K, 56% is lost. Another way to look at these numbers is that, at 800 K, an incident laser beam will have nearly 90% of its energy absorbed after transmitting 40 μm inside a silicon wafer; therefore, the silicon becomes essentially opaque at 800 K. More importantly, as the laser energy is absorbed, it could further increase the temperature and thus more laser energy absorption, leading to the Avalanche Absorption as discussed in Section 5.1. If the avalanche absorption occurs, the laser energy will be

completely absorbed in a thickness much less than 40 µm even though the initial temperature is 800 K.

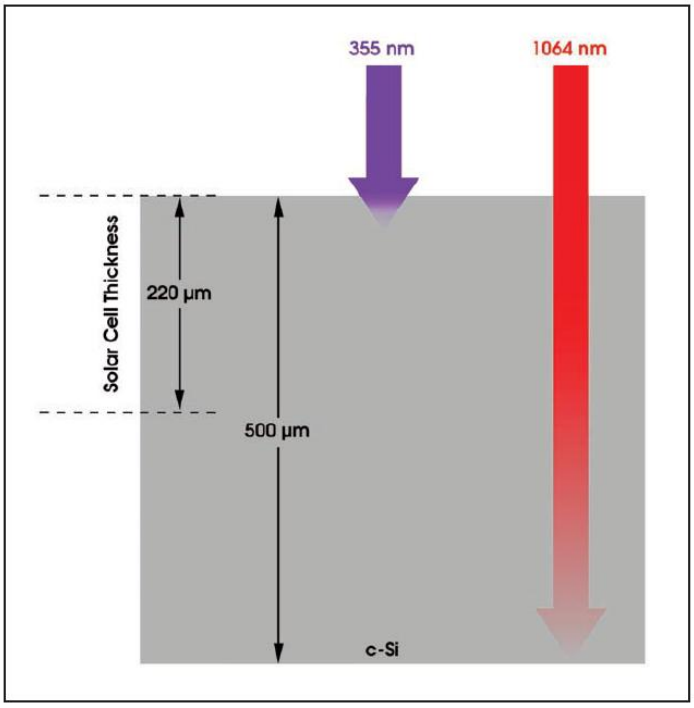

Figure 5.2 Relative penetration depths shown of 355 and 1064 nm laser wavelength (Colville and Dunsky, 2008)

Current systems rely more heavily on diode-pumped solid-state lasers operating at 532 or 355nm because of the significantly higher absorption of crystalline silicon at these shorter wavelengths, which are four to five orders of magnitude stronger than 1064nm, and the concept is shown as Figure 5.2. Taking advantage of temperature dependent property of silicon, we can compensate for the lower absorption of laser energy with 1064-nm wavelength compared with 532 or 355nm. (Colville and Dunsky, 2008)

5.3 Modeling of Avalanche Absorption and Guided Thermal Shock

In (Ohmura et al, 2008), a thermal shock model is developed to explain how cracks are achieved in a patented process called stealth dicing, which is used to cut large wafer into smaller pieces. In the stealth dicing, the crack is created for cutting of silicon wafer. Thermal shock is also generated to propagate crack in the wafer structure. The laser ablation method can be used for successful dicing of the silicon wafer. The laser beam is focused on the surface of the silicon wafer. The wafer surface absorbs the laser energy which causes the ablation of the surface as well as it deforms wafer surface by changing the crystalline structure of silicon. As the laser is focused into the wafer, there is no damage to the surface of the wafer. This eliminates formation of heat affected zones and the debris pollution which occur in conventional laser dicing method

Ohmura et al, 2008 studied the stealth dicing method for 50μm silicon wafer. A permeable nanosecond pulse laser is focused inside the silicon wafer. The pulse energy of 4μJ and the pulse width of the half wave height full width value of 150ns were selected during the experiment. The wafer is moved in horizontal direction and the scribe is made. He estimated that the absorption of 1064nm laser when focused in the silicon wafer depends upon the absorption coefficient of the silicon. It is concluded that absorption coefficient increases with increase in the temperature of the silicon wafer.

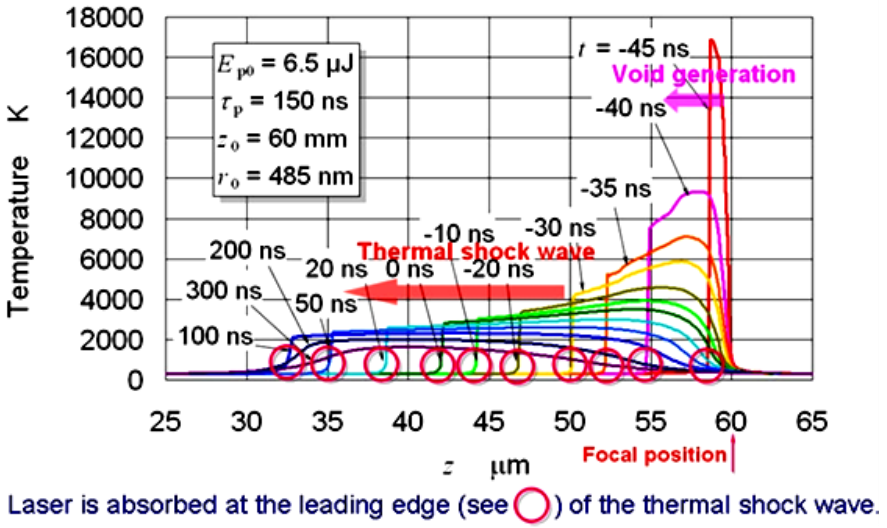

Figure 5.3 Time variation of induced high and narrow temperature field distribution along central axis(ibid)

The mechanism of the SD process is described by a heat transfer and thermal shock model developed by Ohmura et al 2008. This model predicts the induced temperature fields at the focus position, the subsequent thermal shock front, and the avalanche absorption at the thermal shock front shown in Figure 5.3. The void generation is inferred in Figure 5.3, with the evidence of the extremely high and localized temperature rise which is over 16,000 K at the focus position of 60 μm. As shown in Figure 5.3, laser absorption begins suddenly at a depth of z=60 μm at about t=-45ns, and then a void suddenly appears (on-set of avalanche absorption) and a very high and narrow temperature field over 16,000 K is induced. This extremely high temperature field constitutes a thermal shock wave, propagating away. However, as the laser beam is irradiated from the top, only the wave front moving upward meets the laser beam. At the wave front, the temperature easily rises nearly 800 K at which the laser energy is almost completely absorbed (marked in red circle in Figure 5.3). Because the laser energy is almost completely absorbed at the upward shock front, the shock wave front becomes laser guided, "climbing" up along the laser path toward the top surface until the laser pulse is completed. By controlling the focus position, the final crack front and the

high density dislocation area can be confined beneath the top surface; therefore, no debris generation. The Ohmura model is a typical finite difference model with grids in micron sizes with a fixed laser heat source. The main reason for the model's success is that it considers the temperature dependent optical properties of silicon wafer Figure 5.3.

5.4 Void Formations by Different Focus Positions Using Pulsed Laser

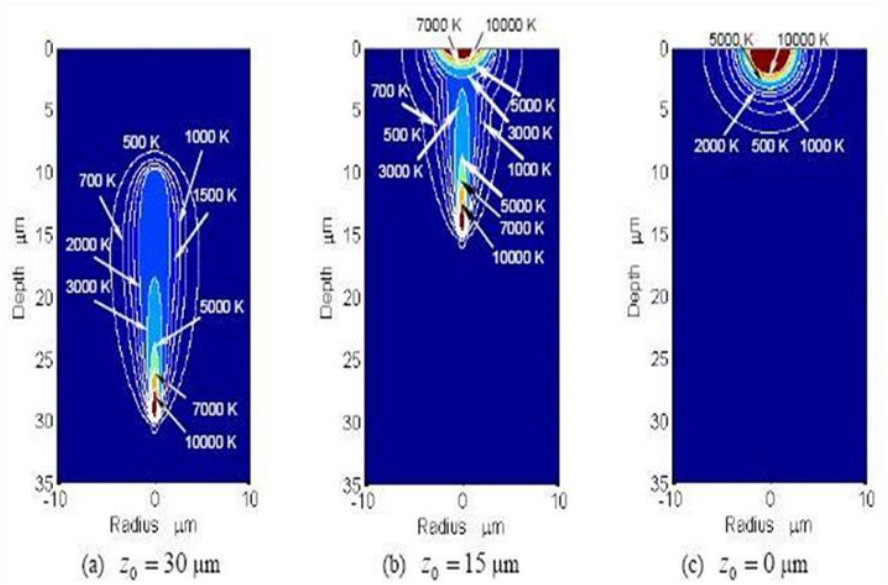

Figure 5.4 Temperature distributions for different focus positions (Ohmura et al,2008)

The Ohmura model also successfully predicts the patterns of temperature fields when focus position is changed, as shown in Figure 5.4. In the cases of Figure 5.4b and 5.4c, where focus positions are at 15 μm and 0 μm (at the surface), the void formation and locations are drastically different. As shown in Figure 5.4b, if the focus position is not deep enough and the thermal shock front arrives at the top surface before the laser pulse is completed, the remainder of the laser energy will be absorbed at the surface, creating a surface groove. Finally, if the focus position is at the top surface, then the avalanche absorption only occurs at the surface to induce a surface groove. The case of Figure 5.4c indicates a probable process that can be explored for edge isolation purposes. As a result, the laser cannot be in focused too deep into the substrate. For laser edge isolation, the condition shown in Figure 5.4c should be maintained. For CW laser edge isolation, it is important to explore a groove as deep as possible before the phenomenon shown in Figure 5.4b.

5.5 Prediction of Depth of Groove Using A Heat Conduction Welding Model

In order to achieve high shunt resistances, the laser edge isolation grooves need to be deep enough to to isolate p-type and n-type silicon electrically. The groove depth varies with change in speed and laser power. Using an adaptation of a 2-D heat conduction keyhole laser welding model, we are able to predict the groove depth which is important to edge isolation. In additon, a particular groove depth can be achieved by manipulating the corresponding process parameters. (Lankalapalli, Tu, *et al.*, 1996) During the welding processing, a keyhole surrounded by molten material is formed after the laser striking the substrate. Then the molten material will fill up the keyhole once the surface tension overcomes the decreased vapor pressure , creating a weld. If the power density at the surface is high enough, the vapor pressure inside the keyhole will increase to a point where it will eject molten material, creating a weld defect called underfill. During the welding process, the power density can be increased by focusing the laser beam near the surface, enhancing this effect and creating a groove instead of a weld. Another way to do it is that the molten material can be blown away with the help of pressurized gas or water jet. So even though this model is developed for predicting the depth of welding process, it can be used to predict the depth achieved during scribing process.

This model has been previously used to predict welding depths of different materials at higher speeds (Lankalapalli, Tu, *et al.*, 1996 and Paleocrassas and Tu, 2007). The general idea of the model is to calculate the heat conduction over an infinitesimally thin layer of thickness (depth) dz at a specific distance from the top of the surface, as shown in Figure 5.5. To make the model more computatuinally efficient, several assumptions have been made. The first assumption is that the walls of the keyhole within this layer are straight and cylindrical to the surface so that heat conducted in the z-direction is much less than the heat conducted in the radial direction. Therefore, a conical keyhole can be divided into an cylindrical heat sources of varying radii, moving together at a constant speed in each of these thin layers. Also, it is assumed the 100% of the laser power is absorbed in the keyhole.

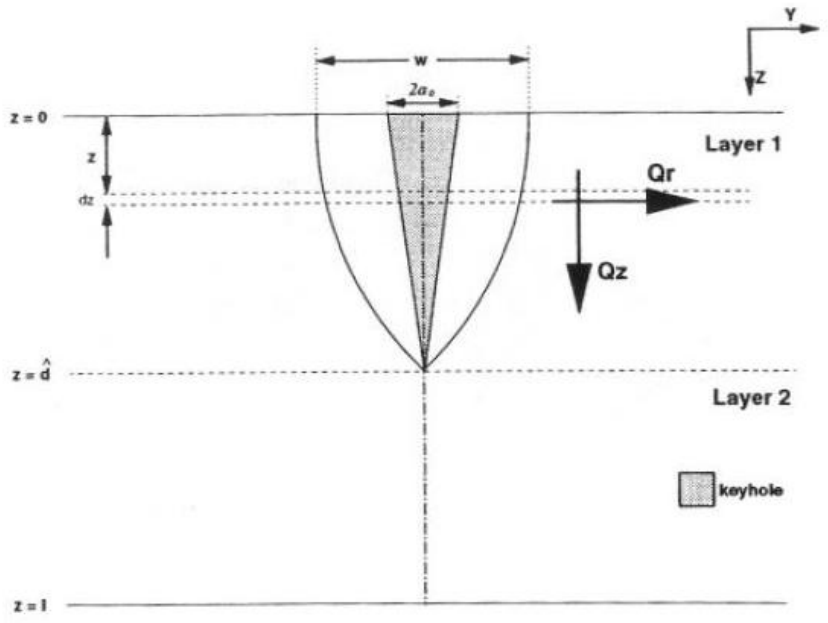

Figure 5.5 Keyhole Profile (Lankalapalli, Tu, *et al.*, 1996)

Another assumption made is that there is a quasi-steady state environment in which a cylindrical surface of radius a, at uniform temperature T_V, is moving with a constant speed, v, along the x direction, in an infinite medium initially at constant temperature, T_0. Finally, assuming that the thermal properties of the medium are constant and that the axis of the cylindrical surface passes through the origin of the coordinate system, the governing differential equations and boundary conditions for the temperature distribution can be written as:

$$\frac{\partial^2 T}{\partial x^2} + \frac{\partial^2 T}{\partial y^2} + \frac{v}{\alpha}\frac{\partial T}{\partial x} = 0 \quad \text{.....(5.1)}$$

$$T = T_V \text{ at } x^2 + y^2 = a^2 \quad \text{.....(5.2)}$$

$$T(x, y) \to T_0 \text{ as } x \to \pm\infty \text{ and y} \to \pm\infty \quad \text{.....(5.3)}$$

where x and y are the surface coordinates, z is the depth coordinate, a is the keyhole radius, v is the welding speed, α is the thermal diffusivity, T_0 is the initial temperature and T_V is the vaporization temperature of the material (Carslaw and Jaeger, 1962).

After several derivations, the following equation which estimates penetration was found as (Lankalapalli, Tu, *et al.*, 1996)

$$d = \frac{P_i}{k(T_V - T_0)} \frac{1}{\sum_{i=1}^{10} \frac{c_i}{i} (Pe_0)^{i-1}} \quad \text{.....(5.4)}$$

where k is the thermal conductivity of the material and c_i are coefficients to a polynomial fit to the equation that was evaluated numerically for 100 different values of Pe in the operating range of 0.0125 - 0.75

$$g(Pe) = \int_0^{2\pi} G(\theta, Pe) d\theta = C_1 + C_2 Pe + C_3 Pe^2 + C_4 Pe^3 \quad \text{.....(5.5)}$$

where

$$G(\theta, Pe) = -Pe * e^{(-Pe\cos\theta)} * \left[\sum_{n=0}^{\infty} \varepsilon_n I_n(Pe) \cos(n\theta) \left(\frac{n}{Pe} - \frac{K_{n+1}(Pe)}{K_n(Pe)} - \cos\theta \right) \right] = \frac{\partial}{\partial r^*} \left(\frac{T_V - T}{T_V - T_0} \right) \Big|_{r^*=1} \quad \text{.....(5.6)}$$

where

$$\frac{T_V - T}{T_V - T_0} = 1 - e^{(-Pe*r^* \cos\theta)} * \sum_{n=0}^{\infty} \varepsilon_n \frac{I_n(Pe)}{K_n(Pe)} K_n(Pe*r^*)\cos(n\theta) \quad \text{.....(5.7)}$$

is the closed-form solution in polar coordinates (r,θ) of the aforementioned governing differential equation with the specified boundary conditions for the temperature distribution, where Pe = v*a / (2α) is the Péclet number, r^* = r/a is the normalized radial coordinate, ε_n = 1 for n = 0 and 2 for n ≥ 1, I_n is a modified Bessel function of the first kind, of order n and K_n is a modified Bessel function of the second kind of order n.

During the welding process, the material melts inside the weld area. This molten material can be blown away with the help of pressurized assist gas or water jet. So even though this model is developed for predicting the depth of welding process, it can be used to predict the depth achieved during scribing process.

5.6 Hypothesis of Temperature Manipulation of Crystalline Silicon

Due to temperature dependent optical properties of crystalline silicon that the absorption of laser energy by silicon increases at elevated temperatures, the lower absorption of laser energy of 1064-nm wavelength can be compensated, and therefore a deeper edge isolation groove can be created by preheating the silicon to specific temperature.

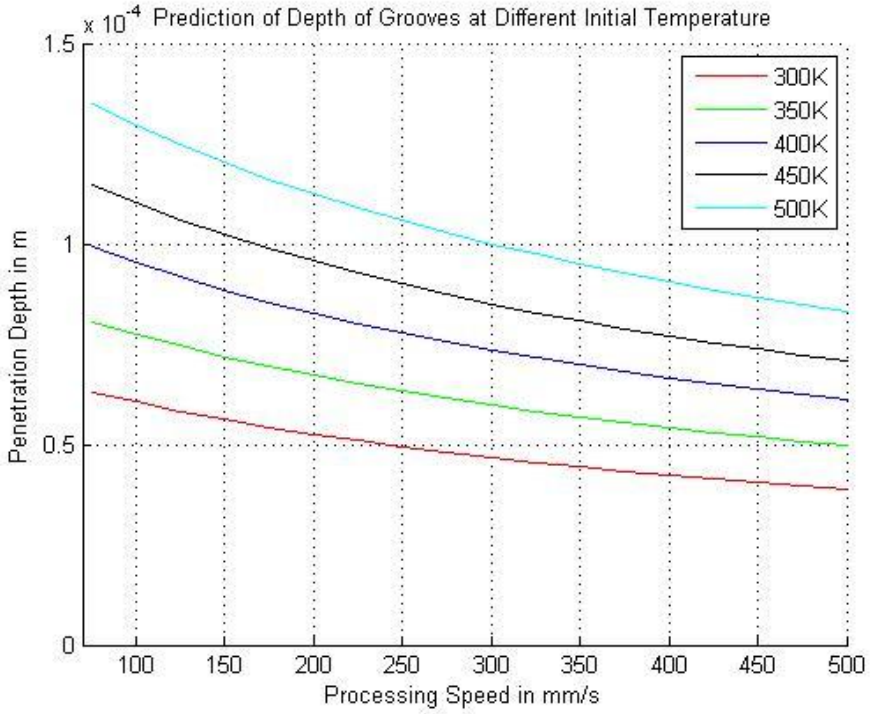

Figure 5.6 Prediction of Variation of Depth in Silicon at Different Initial Temperature

Figure 5.6 shows the predicted variation of depth in Silicon, at different initial temperatures (T= 300K – 500 K) for a processing speed range of 75-500 mm/s using the 2-D welding model. Depth values were calculated using equation 5.4 (see Appendix for MATLAB model).

$$d = \frac{P_i}{k(T_V - T_0)} \frac{1}{\sum_{i=1}^{10} \frac{c_i}{i} (Pe_0)^{i-1}} \quad \text{.....(5.4)}$$

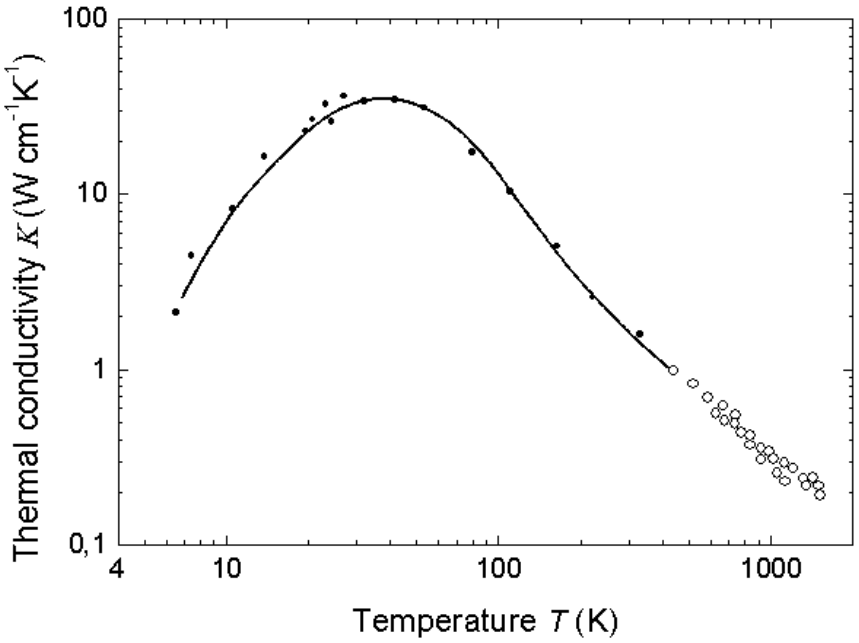

Figure 5.7 Temperature dependence of thermal conductivity for high purity Si.(Glassbrenner and Slack, 1964)

From Figure 5.7 it indicates that the thermal conductivity k is the function of temperature T, so once the initial temperature of the silicon changes, the material has different k. Silicon has the highest thermal conductivity at 40K; after that, when the temperature goes higher, the k value becomes lower and lower. In equation 5.4, the value of d is determined by the product of k and (T_V -T_0) if other terms are constant. The product of k and (T_V -T_0) becomes smaller at the temperature higher than 40K, so it makes the depth become larger. Another explanation in terms of physics is that due to the lower thermal conductivity, the heat transferring across materials is less, so at the local spot more substrate is melted and vaporized by laser.

During the welding process, the material melts inside the weld area. This molten material can be blown away with the help of pressurized assist gas or water jet. So even though this model is developed for predicting the depth of welding process, it can be used to predict the depth achieved during scribing process.

6 EXPERIMENTAL APPARATUS

Figure 6.1 300 W Ytterbium, Single-mode fiber laser power unit

A 300 W Ytterbium, Single-Mode, Fiber Laser (Figure 6.1) is used for this research. A NEMA two-phase 220V outlet provides electric power to the laser. Its near infrared (1,075 nm) beam is fiber deliverable and comes out of the collimator as a cylindrical 5 mm beam. The laser beam quality is near Gaussian ($M^2 \sim 1.04$).

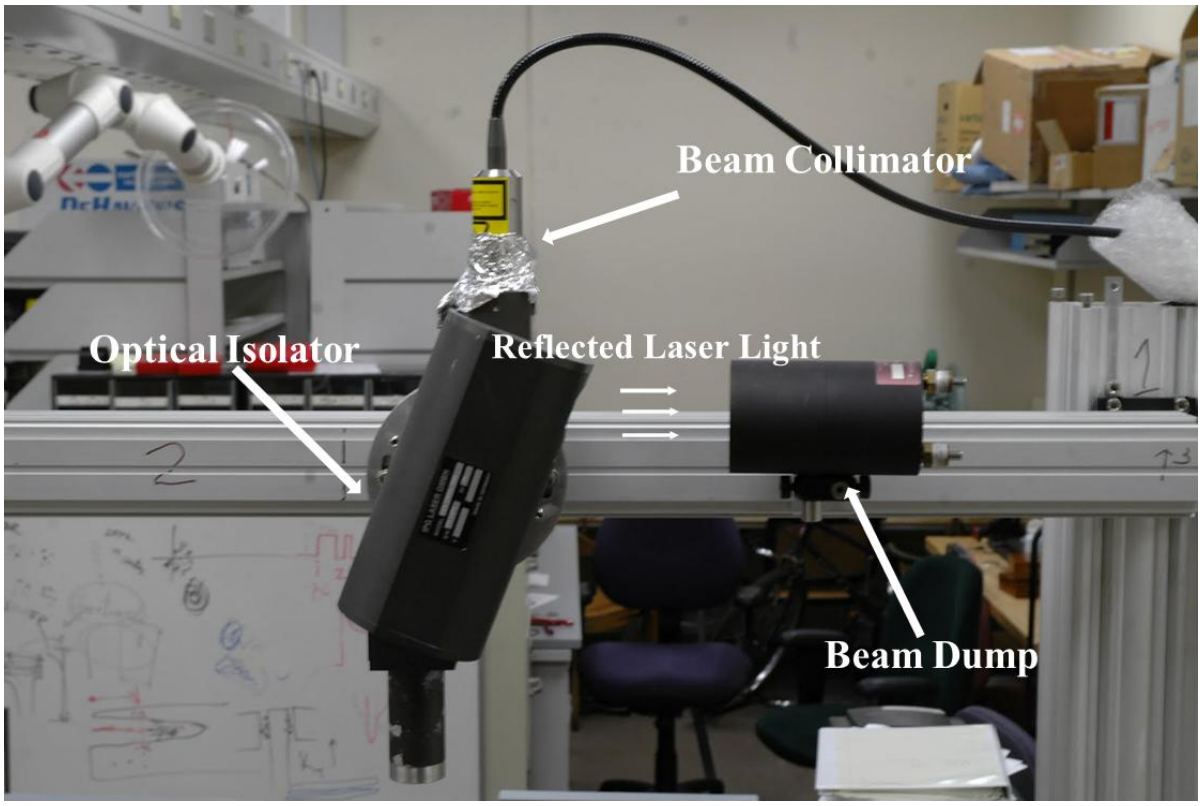

Figure 6.2 Optical isolator connection to collimator, used to divert away reflected laser light into a beam dump

An optical isolator (shown in Figure 6.2) was attached to the collimator and is used to divert any reflected light away from the collimator in order to avoid damage to the fiber due the high reflectivity of aluminum. The beam diameter and beam quality were modified slightly (beam diameter~7 mm, $M^2 \sim 1.15$).

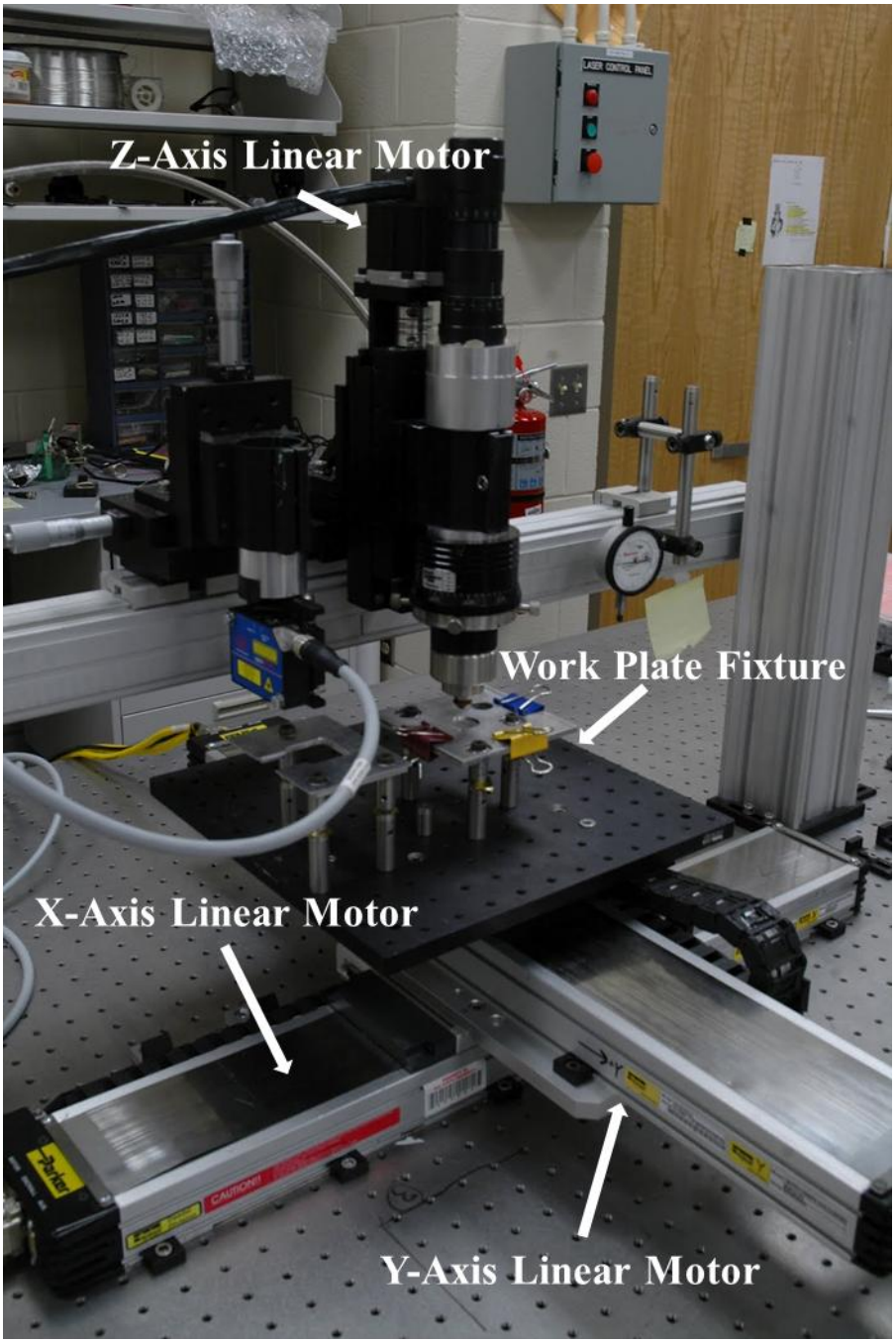

Figure 6.3 XYZ Linear motors with attached work plate fixture

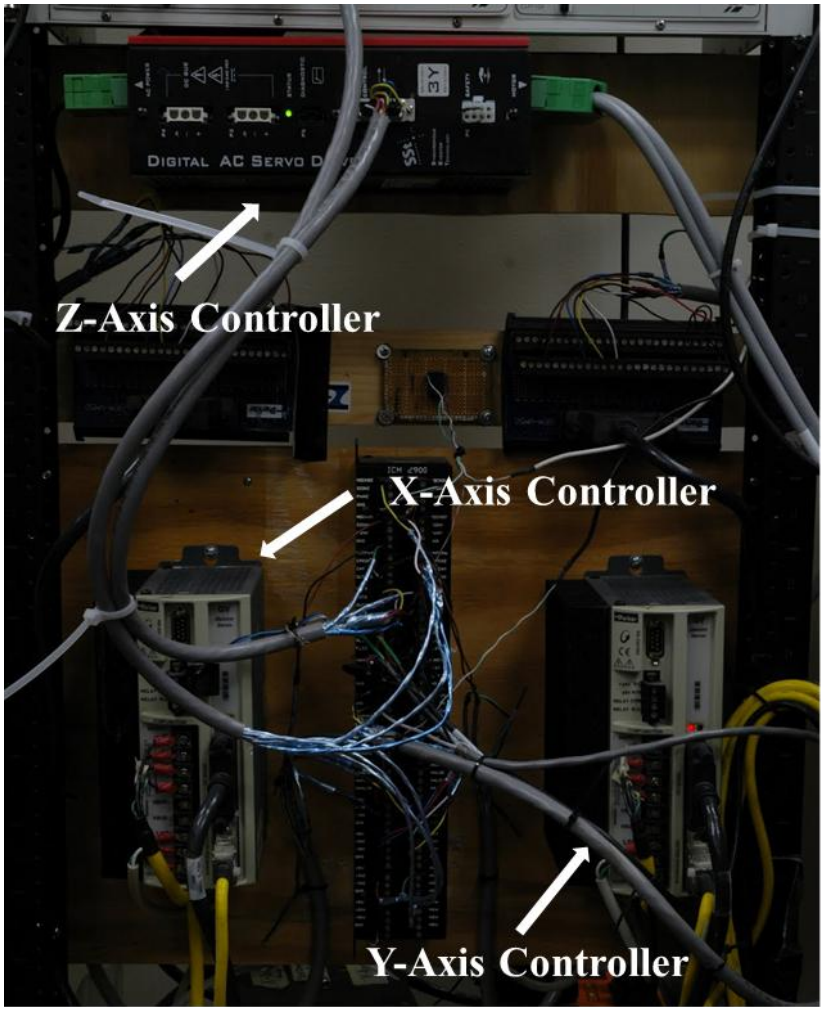

Figure 6.4 Galil XYZ axes motion controllers

The Parker Automation XY linear motors (Figure 6.3) are used to move the workpieces and the Z linear motor is used to move the laser head setup, as well as the focusing of the laser beam; they are controlled by the Galil XYZ axes motion controllers (Figure 6.4). For the XY linear motors, they have a resolution of 0.5 μm and a range of 1 m. The maximum acceleration and deceleration is ± 2 g's and maximum speed is 1.5 m/s. On the other hand, the Z linear motor has a resolution of 0.63 μm and a range of 0.11m. The maximum acceleration and deceleration is ± 2 g's and maximum speed is 0.5 m/s.

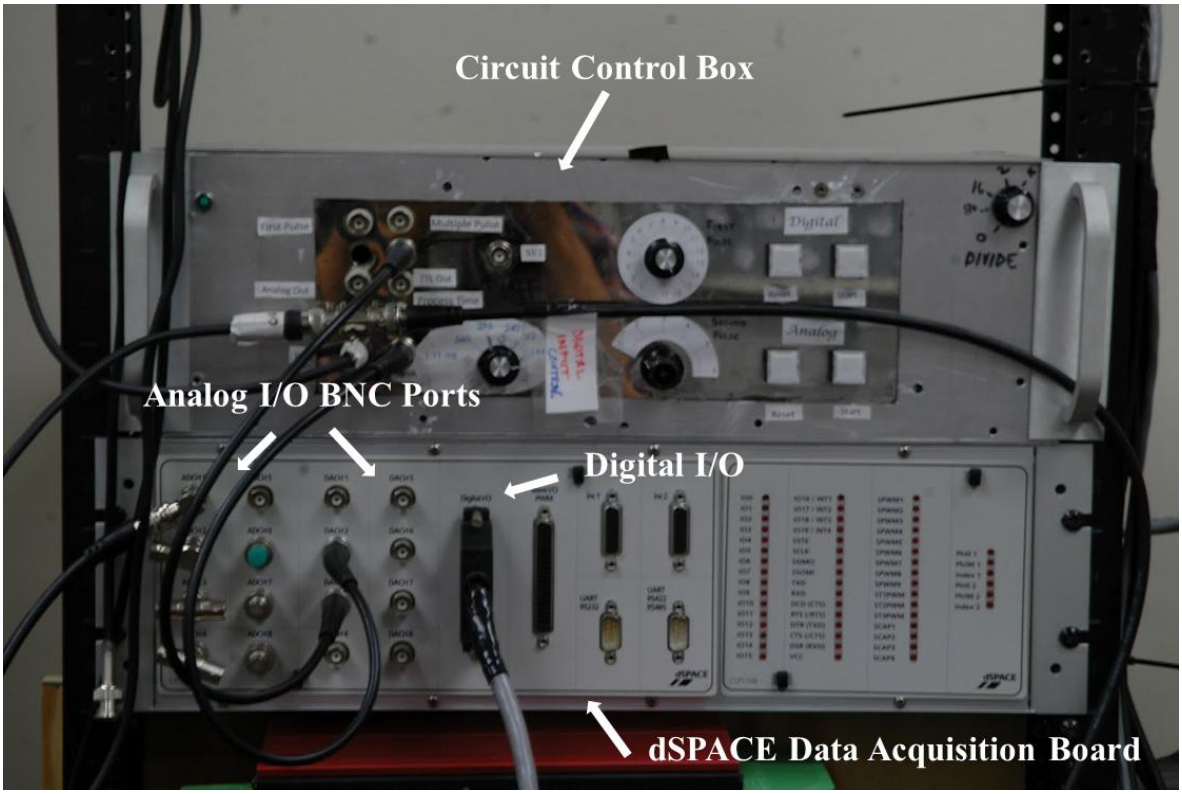

Figure 6.5 dSPACE 4.0 data acquisition system and circuit control box

The data acquisition system used is dSPACE 4.0 (Figure 6.5). It is mainly used as an external control for the laser and for acquiring data from sensors (photodiode). This helps automate the operation of the laser. Simulink is used to create different operation schemes and can be synchronized with the movement of the linear motors.

The circuit control box (Figure 6.5) is designed to control single and multiple pulses of the laser. Outputs are connected to BNC connectors for monitoring of the process time, the first pulse length, subsequent pulse lengths, and the overall output. Manual set and reset push buttons are connected as well as BNC connects for set and reset for computer control.

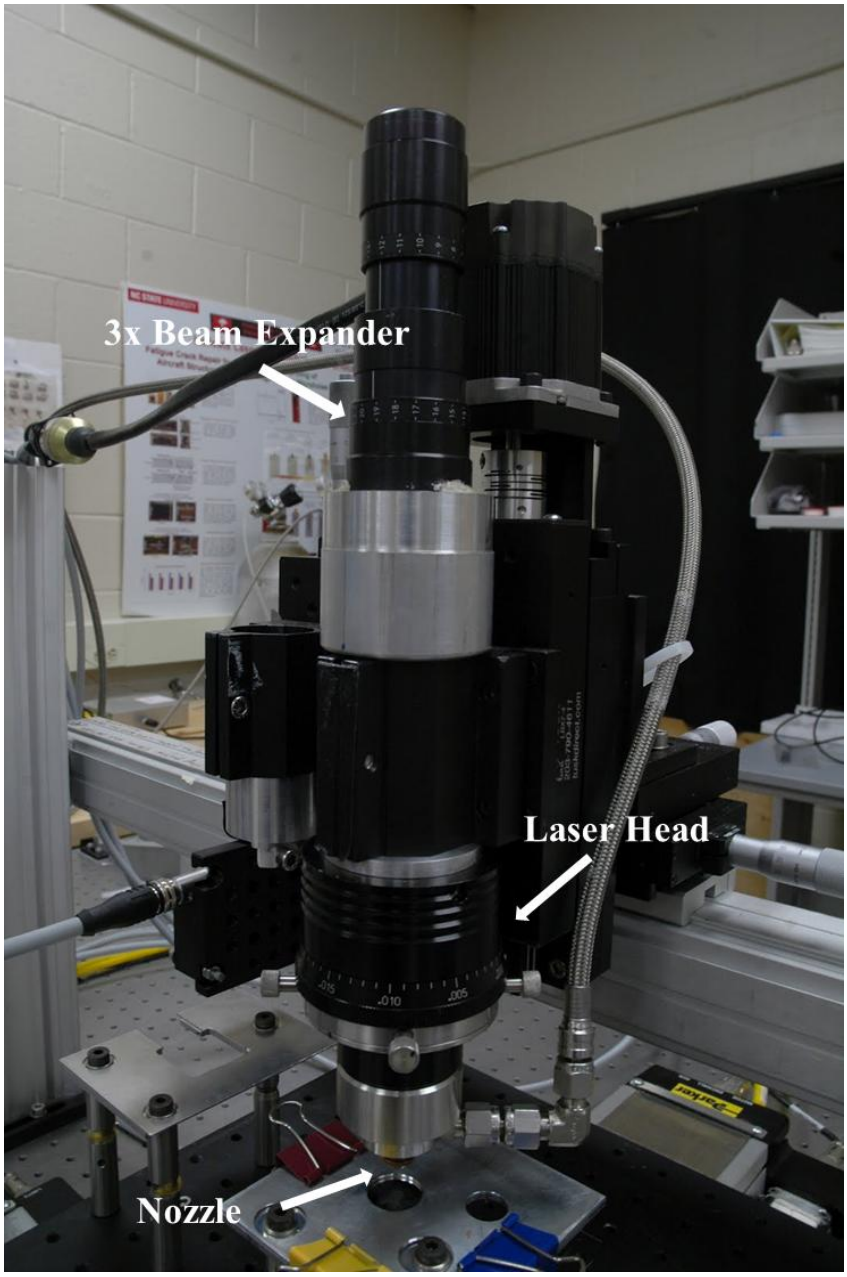

Figure 6.6 Beam expander and laser head setup

A 3x beam expander is used in combination with the 100.1 mm OptoSigma triplet lens to obtain a minimum focus spot size of 12.01 μm. Equation 6.1 shows how to calculate the minimum spot size.

$$\text{Spot Size} = \frac{Lens\ Focal\ Length}{Collimator\ Optics\ Focal\ Length \times Beam\ Expantion\ Fctor} \times Fiber\ Diameter = \frac{100.1mm}{25mm \times 3} \times 9\mu m = 12.01\mu m$$

……(6.1)

Figure 6.6 shows the optical setup. The laser beam is centered with respect to the beam expander and the laser head. The laser head contains the focusing triplet and can be adjusted using the outer ring. At the bottom of the cutting head there is a chamber that allows for shielding to flow out through the welding nozzle. This chamber is sealed by a special cover glass and a rubber gasket.

Figure 6.7 Tektronix 3012B oscilloscope

For data acquisition, a Tektronix 3012B oscilloscope was used, shown in Figure 6.7. It has two input channels and the sampling rate capabilities go up to 100 MHz. It always acquires 10,000 samples and the sampling rate is determined by the time range that is chosen.

Figure 6.8 Zeiss Inverted Microscope

The Zeiss (Figure 6.8) inverted microscope was used to enlarge all the grooves cross-sections and obtain pictures. There are a number of different magnifications that can be obtained. The current objectives are 2.5x, 8x, 16x, 40x and 80x. There is also an additional 2x magnification factor that can be multiplied to these aforementioned objective magnifications. Also, the eyepieces provide the user with a 10x magnification. Therefore, the maximum magnification that can be obtained is 1600x.

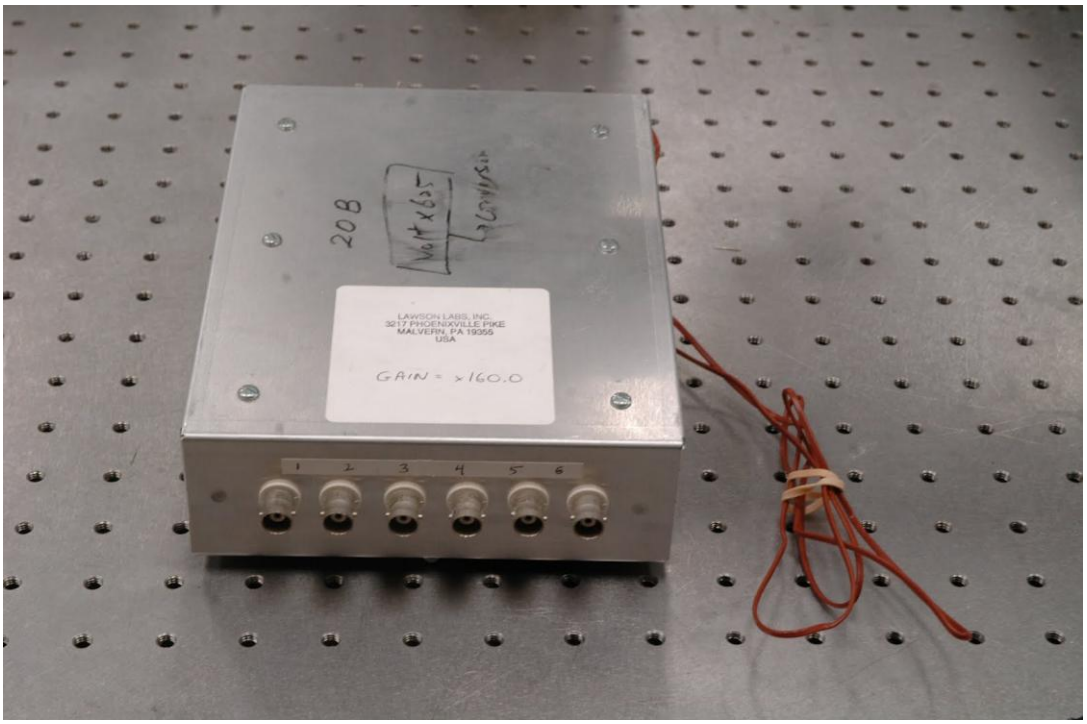

Figure 6.9 K-type thermocouple

In this research thermocouples shown in Figure 6.9 are used to measure the temperature of solar cell when it is preheated. The type of thermocouple used is a K-type thermocouple from Omega Engineering Inc. These are bonded to a wire by a high temperature, thermally conductive, and electrically insulating cement, also from Omega Engineering Inc. These thermocouples are connected to a custom low noise thermocouple amplifier purchased from Lawson Labs to amplify the signal of the thermocouples. The output from the amplifier is connected to a D-Space DS1104 real-time data acquisition system, and this is the instrument that actually records the "temperature", which is actually just a voltage from the amplifier. A Simulink model is used to convert the voltage to temperature in the D-Space software.

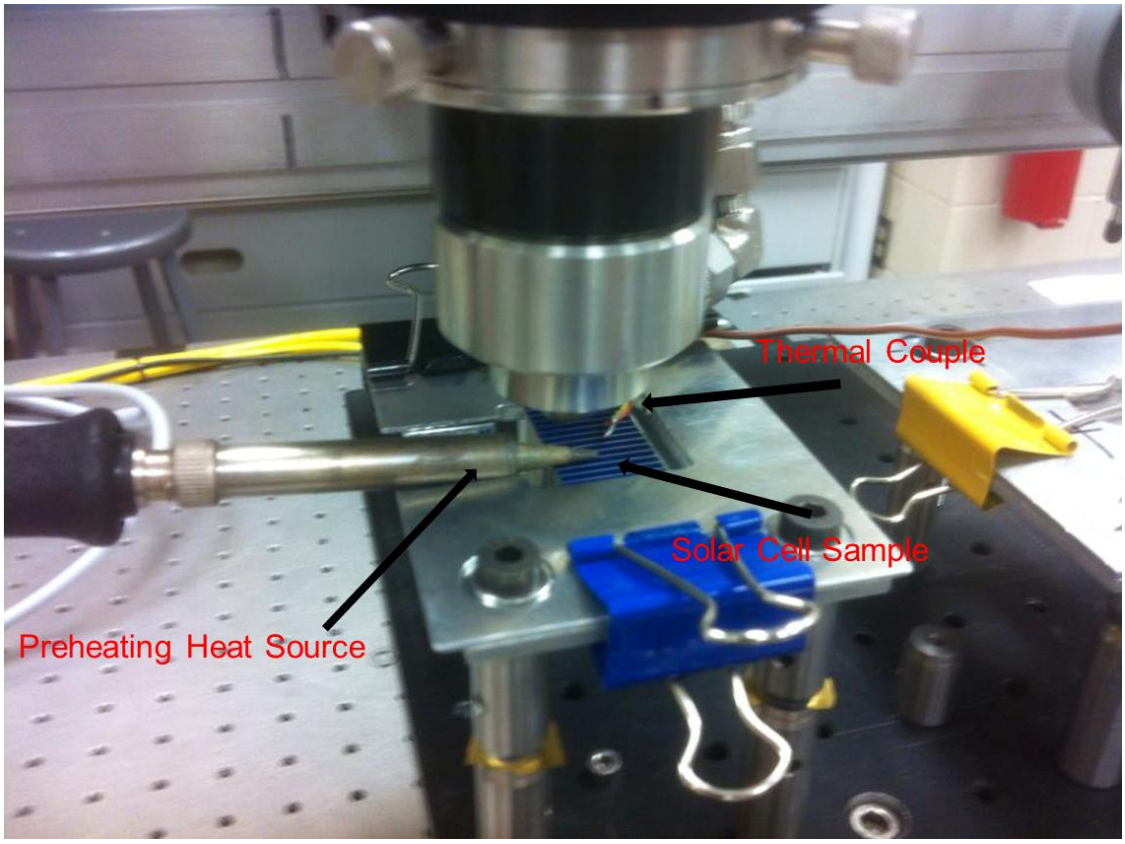

Figure 6.10 Experimental Setup

The way we conducted the experiments with different initial temperature was that the soldering iron was attached at the front side of the solar cell when it was on the servo table, and then thermocouple was used to measure the temperature from the top of solar cell. When solar cell was heated up to certain temperature, the soldering iron and thermocouple were removed away immediately and then a groove was made. The procedure was repeated for each groove to maintain target temperature for accuracy.

7 EXPERIMENTAL PROCEDURES

The experimental procedures to achieve the research objectives are as following

- Study of silicon optical properties
- Modeling the laser scribing process
- Experimental investigation for the effects of temperature control, laser focusing, power and scribing speed

7.1 Transmission test of LASER through Si wafer with different initial temperatures

The experiment was carried out to check the transmission of the LASER through Si wafer with active temperature control. InGaAS photodiode was aligned below the beam expander. First of all, the laser power was set to 10% power (30W) and the photodiode output was checked without placing out Si wafer above the photodiode. Laser power was increased in steps of 5% (15 W) to 100% (300W) and the photodiode out puts were recorded. Next, repeat all the steps with placing Si wafer above the photodiode and the outputs were recorded. Last, repeat all the steps with placing Si wafer above the photodiode and with a preheating source to Si wafer. Initial temperature was changed by heating up the silicon wafer till the temperature reached 400K, and the photodiode out puts were recorded. There were totally three sets of data recorded. For each output curve of photodiode, steady state values were calculated. Depending on these steady state values, the graph was plotted.

7.2 Controlling parameters for the edge isolation process

The edge isolation grooves are done by the laser scribing process, which can be controlled by adjusting various process parameters which include processing speed, laser power, focus position and temperature control. Experiments were done to examine effect of each processing parameter on the edge isolation process. During the experiments, only one processing parameter was changed in order to examine the effect of each processing parameter. An acceptable range of each parameter is determined from the results of these experiments.

7.2.1 Laser Focusing Test

Before conducting experiments, the focus position of the laser beam needed to be determined. A small steel piece with 0.8 mm thickness was chosen to determine the focus position. The plate was sandwiched securely between the aluminum fixtures using the clips. The fixture was supported by 70 mm posts and it was fixed using clamps on the platform. Flatness of the plate in x-y plane was checked by dial gauge till the flatness of 0.0001" was achieved. The height of the surface of the steel plate was calculated from measurements of height gauge and the dial gauge. This height was recorded to determine correct focus position for further experiments. A single pulse of 27.2 μs was selected as an input to the laser. Laser power of 300W was selected during the experiment. First spot was made on the steel plate by adjusting z-position of the laser. After each pulse was shot, focus position was increased by 10 μm. Several spots were made by shooting single pulses. Spot diameters were measured on the inverted microscope. A graph was plotted using spot diameter measurements and corresponding focus position. A suitable focus position was determined from the data points at the tip of the curve.

7.2.2 Different initial temperatures on edge isolation groove

A 2 cm x 4.5 cm solar cell of thickness 220 μm was selected to perform this experiment. The wafer was sandwiched securely between the aluminum fixtures using clamps. The fixture was supported by 70 mm posts and it was fixed using clamps. Flatness of the fixture plate in x-y plane was checked by dial gauge till the flatness of 0.0001" was achieved. The laser power was set to minimum. The minimum power that can be adjusted is 30W with the setup available. Processing speed of 75mm/s was set while performing the experiment. Laser was focused on the surface of the solar cell. Initial temperature was changed by heating up the solar cell till the temperature reached to specific temperature such as 300K (room temperature), 350K, 400K and finally 450K. One groove was created for each initial temperature. Sample was then observed under inverted microscope to determine geometry of the grooves. All the steps were repeated twice to create two more set for comparison to see if repeatable.

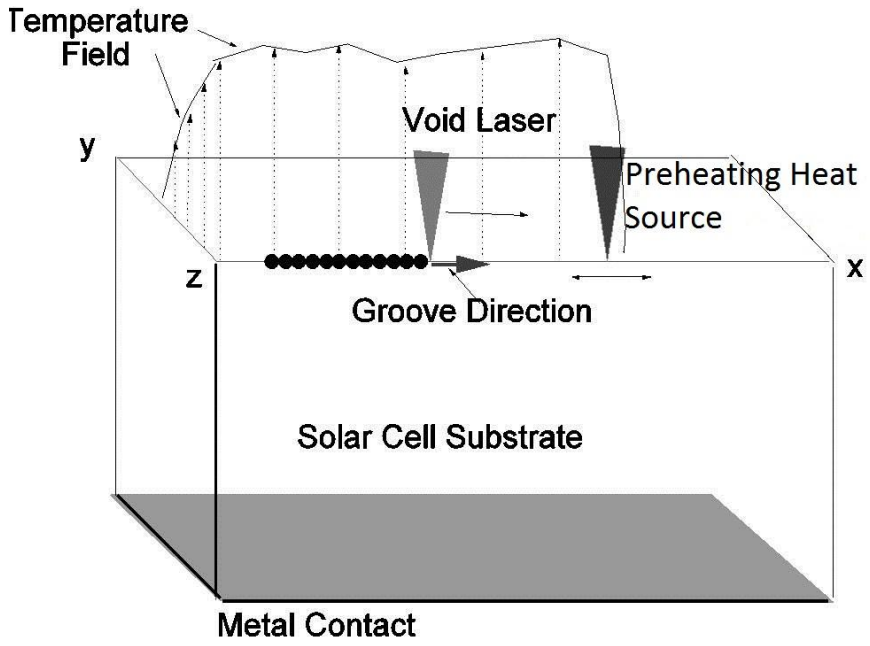

Figure 7.1 Illustration of crack-free edge isolation process with prescribed temperture field

7.2.3 Different power on edge isolation groove

A 2 cm x 4.5 cm solar cell of thickness 220 μm was selected to perform this experiment. The wafer was sandwiched securely between the aluminum fixtures using clamps. The fixture was supported by 70 mm posts and it was fixed using clamps. Flatness of the fixture plate in x-y plane was checked by dial gauge till the flatness of 0.0001" was achieved. The laser power was set to minimum. The minimum power that can be adjusted is 30W with the setup available. Processing speed of 75mm/s was set while performing the experiment. Laser was focused on the surface of the solar cell. The temperature was set to 293K (room temperature). Initially 10% (30W) laser power was selected as it was the minimum power which could be selected with current setup. One groove was created for each power. After creating each groove, power was then increased by 1% (3W) till 20% (60W). Sample was then observed under inverted microscope to determine geometry of the grooves. All the steps were repeated twice to create two more set for comparison to see if repeatable.

7.2.4 Different scribing speed on edge isolation groove

A 2 cm x 4.5 cm solar cell of thickness 220 μm was selected to perform this experiment. The wafer was sandwiched securely between the aluminum fixtures using clamps. The fixture was supported by 70 mm posts and it was fixed using clamps. Flatness of the fixture plate in x-y plane was checked by dial gauge till the flatness of 0.0001" was achieved. The laser power was set to minimum. The minimum power that can be adjusted is 30W with the setup available. Laser was focused on the surface of the solar cell. The temperature was set to 293K (room temperature). Initially scribing speed was selected as 75mm/s and then 100mm/s, then increased by 50mm/s till 500mm/s. Sample was then observed under inverted microscope to determine geometry of the grooves. All the steps were repeated twice to create two more set for comparison to see if repeatable.

8 RESULTS AND DISCUSSION

8.1 The result of transmission of the laser through silicon with different temperature

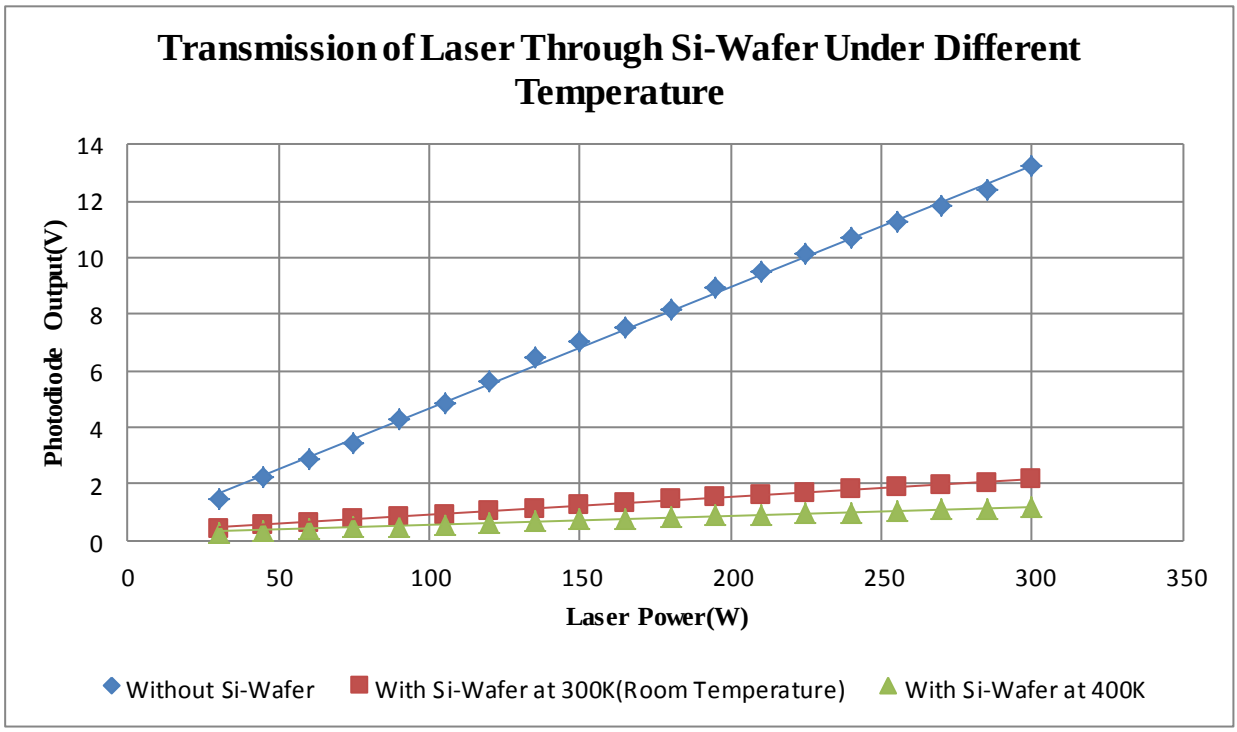

Figure 8.1 Transmission of the laser through silicon wafer under different temperature

According to Figure 8.1, the result of transmission test proves the hypothesis that silicon has the temperature dependent optical property that when the temperature is higher, the silicon would absorb more optical energy. The way it is interpreted is that, first, the ratio of without Si-wafer to with Si-wafer at 300K is higher rather than constant when the power is increased, which means that at higher power the silicon absorbs more power, so less power penetrates through the silicon. The reason is that the higher power induces higher temperature field in silicon when laser power is incident in, and then the higher temperature field results in higher absorption. Second, at 400K the photodiode output is less than 300K, which means more power is absorbed at 400K. Therefore, higher initial temperature can be a tool to enhance the absorption of laser energy without using higher laser power.

8.2 Effect of different powers on the grooves

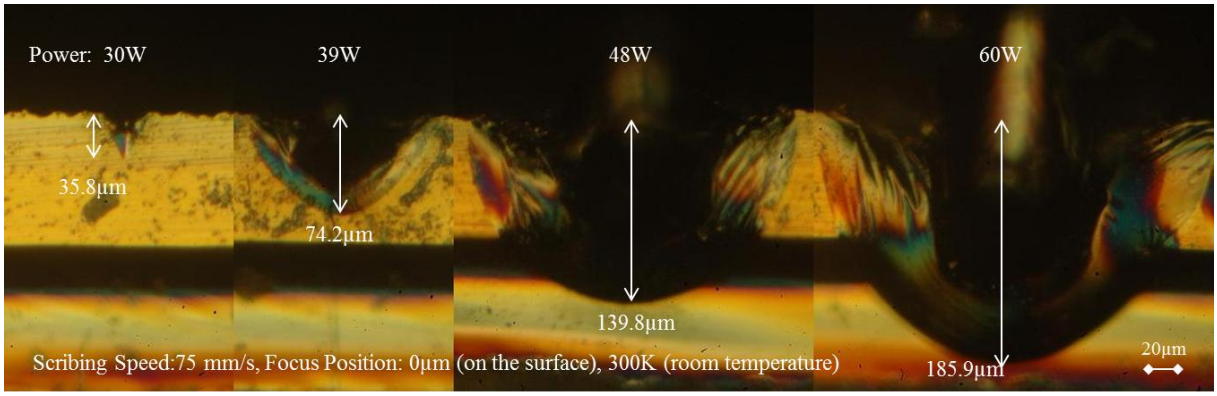

Figure 8.2 Depth of the grooves at different powers on the solar cell

As shown in Figure 8.2, when the power of the laser is increased, the width of the groove also increases. However, at the powers more than 39W, we can clearly see the presence of cracks, which are undesirable to edge isolation and can result in failure of solar cell. It proves that the micro cracks can be form in longer laser wavelengths processing. (Colville and Dunsky, 2008) The reason the cracks formed is that the localized energy absorption induces a sharp temperature and high thermal stress, and the thermal stress overcomes strength of material, causing the crack. From this experiment we learn that to have crack-free edge isolation the laser power has to be set as low as possible.

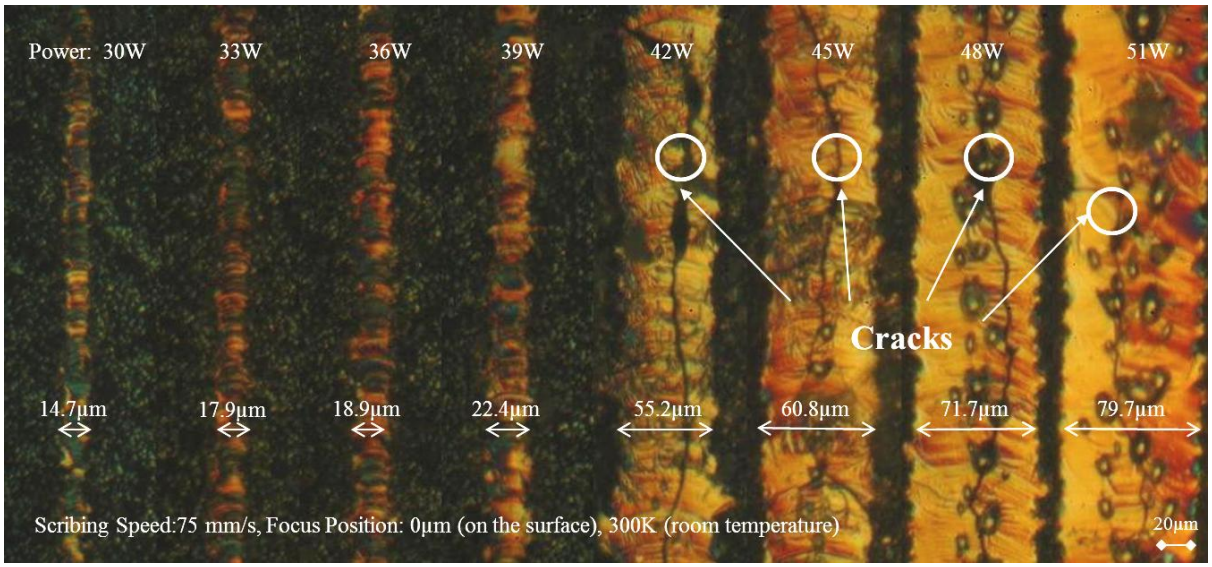

Figure 8.3 Width of the grooves at different powers on the solar cell

As shown in Figure 8.3, when the power of the laser is increased, the width of the groove also increases. However, at the powers more than 39W, we can clearly see the presence of cracks, which are undesirable to edge isolation and can result in failure of solar cell. It proves that the micro cracks can be form in longer laser wavelengths processing. (Colville and Dunsky, 2008) The reason the cracks formed is that the localized energy absorption induces a sharp temperature and high thermal stress, and the thermal stress overcomes strength of material, causing the crack. From this experiment we learn that to have crack-free edge isolation the laser power has to be set as low as possible.

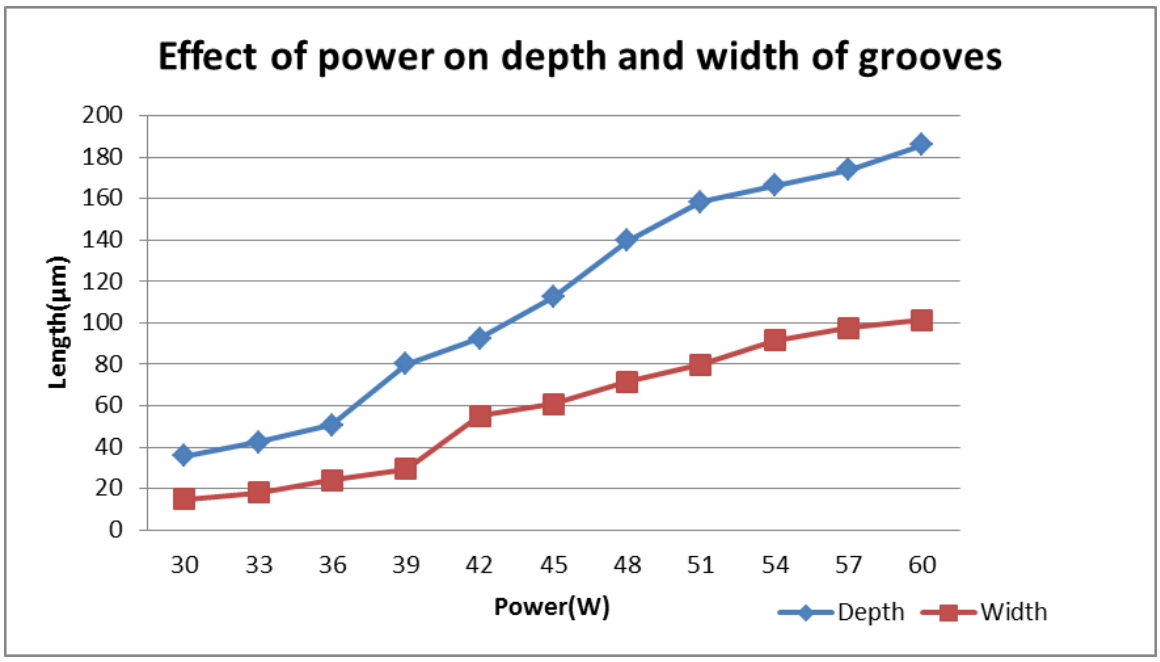

Figure 8.4 Effect of power on depth and width of the groove

As it is mentioned above, when the power of the laser is increased, the width and depth of the groove also increases. In Figure 8.4 it shows how the increasing power influences the depth and width of the grooves. For the change of width, there is a sudden jump between 39W and 42W; the width at 42W is two times of the width at 39W. On the other hand, the sudden jump happened between 36W and 39W on the depth of the groove, and the value at 39W approximately one and half times at 36W. This phenomenon implies that from 36W to 42W there must have been a threshold condition of stronger avalanche absorption; the thermal absorption coefficient of silicon is different before and after the threshold condition.

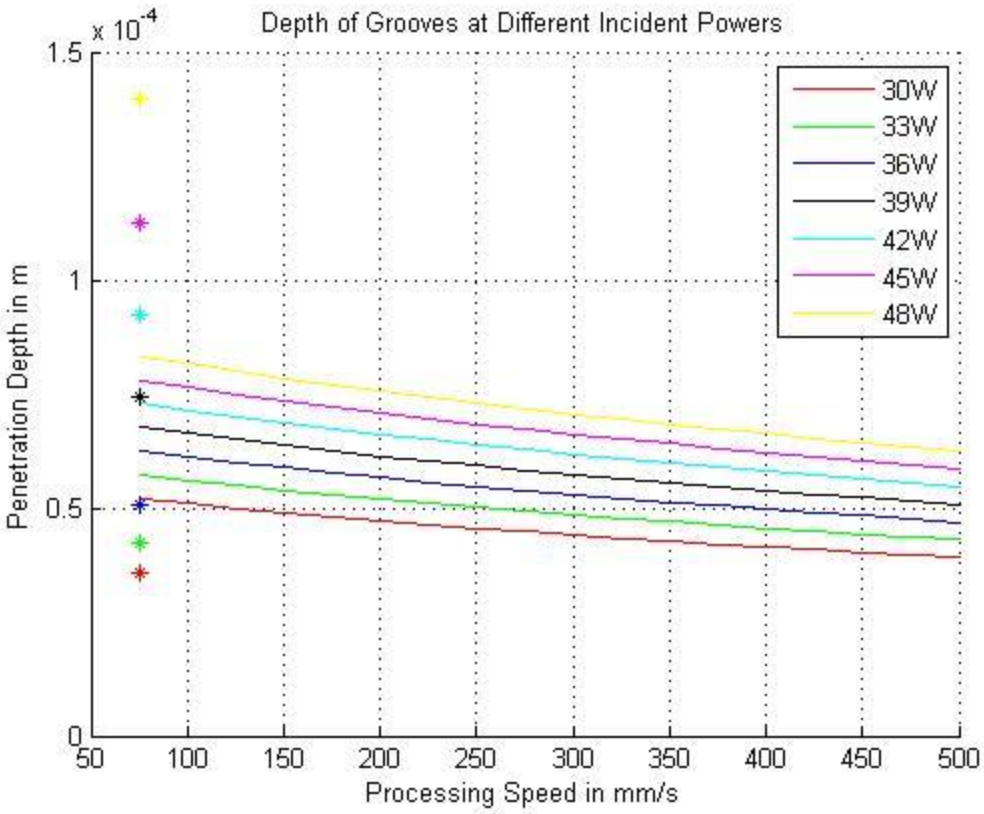

Figure 8.5 Variation of penetration depth of solar cell at different power settings

Figure.8.5 shows the differences between the experimental results cell at different power settings and the prediction of the 2-D model. The star marks in different colors represent the experimental results, and the curves represent the 2-D model. When the power is lower than 36W, the result is predictable. The reason why the experimental results below 36W is smaller than 2-D model is because the model is assumed that 100% of the laser power is absorbed in the keyhole, but the absorption of silicon wafer is not 100% at room temperature. When the power is higher than 39W, the results become unpredictable.

8.3 Effect of different initial temperatures on the grooves

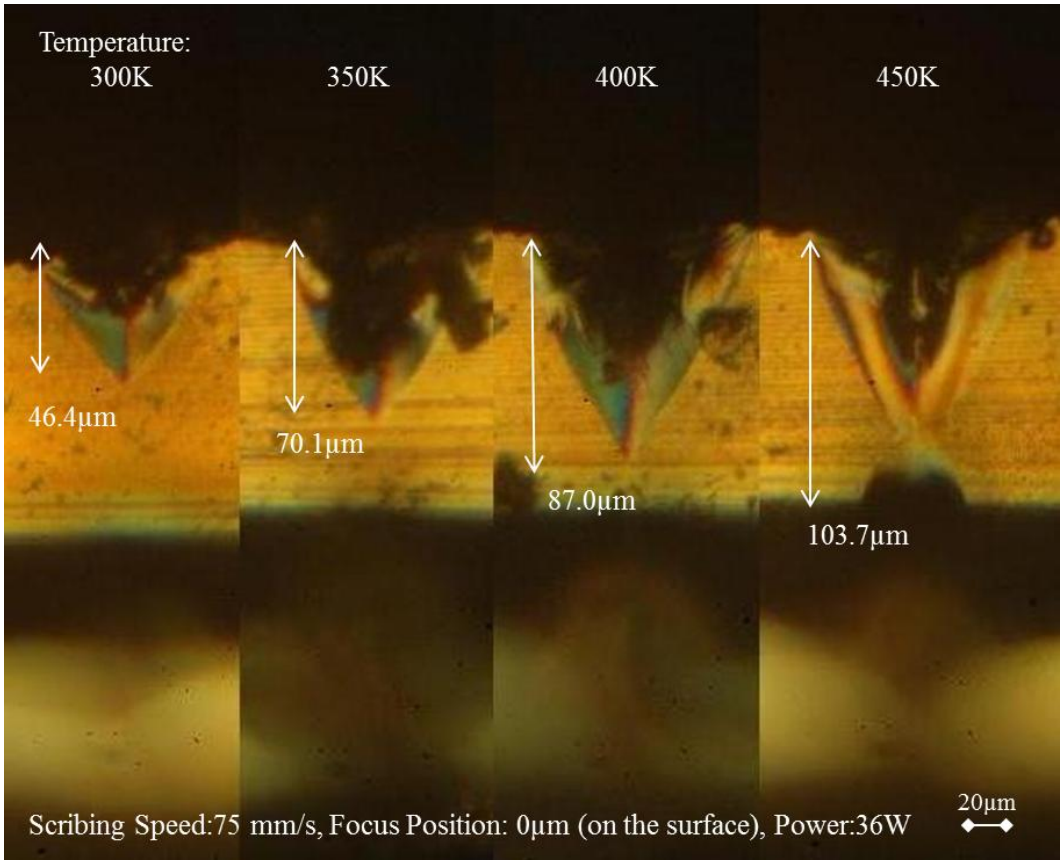

Figure 8.6 Depth of the grooves at different initial temperature on the solar cell

Figure 8.6 shows how the different initial temperature influences the grooves. It clearly indicates that the higher the initial temperature is, the deeper the groove is, and it is absolutely a strong evidence of the temperature dependent property. When the temperature is increased, the contour of the groove does not change very much; it still maintains the conical shape.

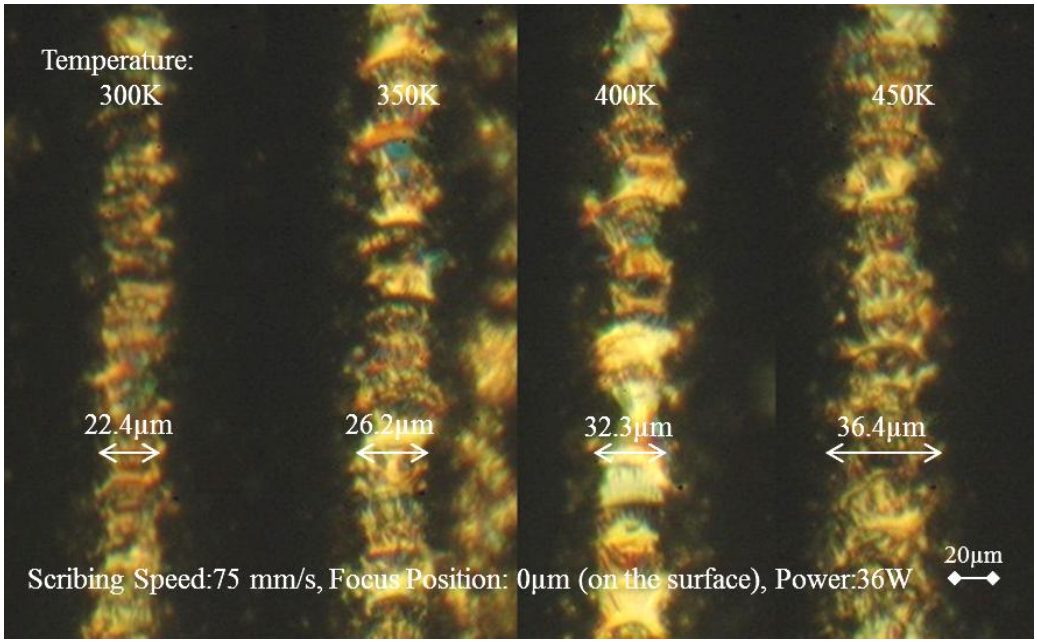

Figure 8.7 Width of the grooves at different initial temperature on the solar cell

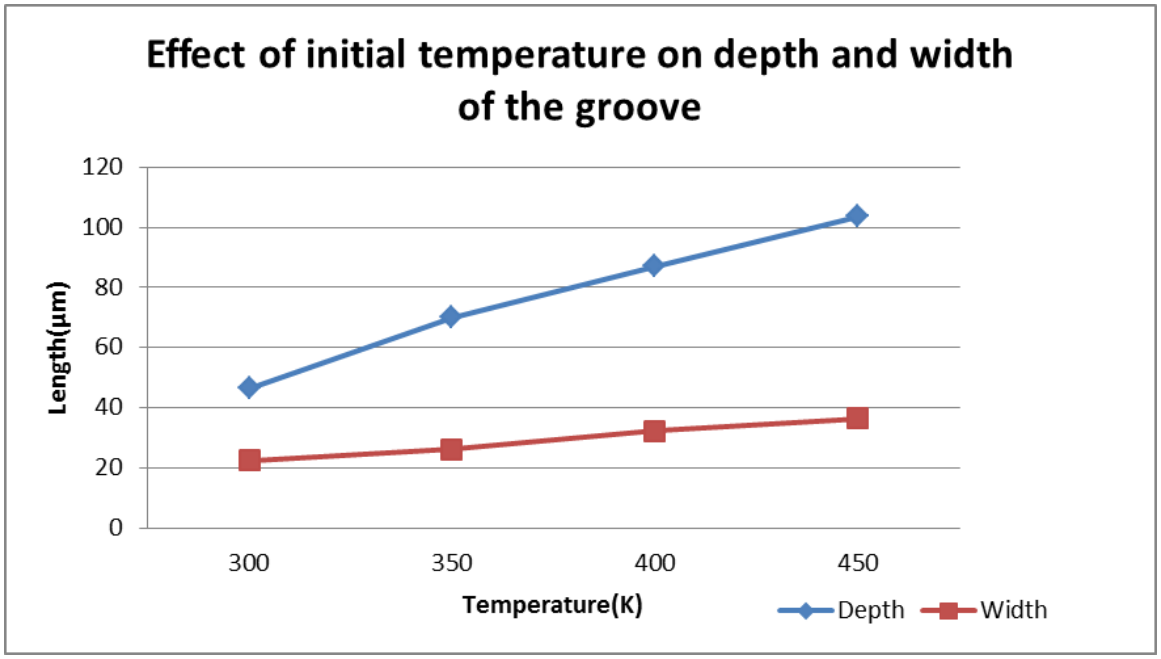

Figure 8.8 Effect of initial temperature on depth and width of the groove

As we can see in Figure 8.7, there is no presence of crack at each different position, so the change of initial temperature is not the factor to cause this problem. In Figure 8.8 above, it shows the relationship between depth and width when the temperature is increased. Although the depth and the width both increase when the temperature is higher, the width does not rise as much as the depth. The depth at 450K is more than twice of the depth at 300K, but the width in the same condition is less than twice. The depth of the groove increases because the laser absorption coefficient is higher at higher temperature the initial formation of keyhole is deeper, which means less laser power penetrates through the solar cell. The result is consistent with the transmission test.

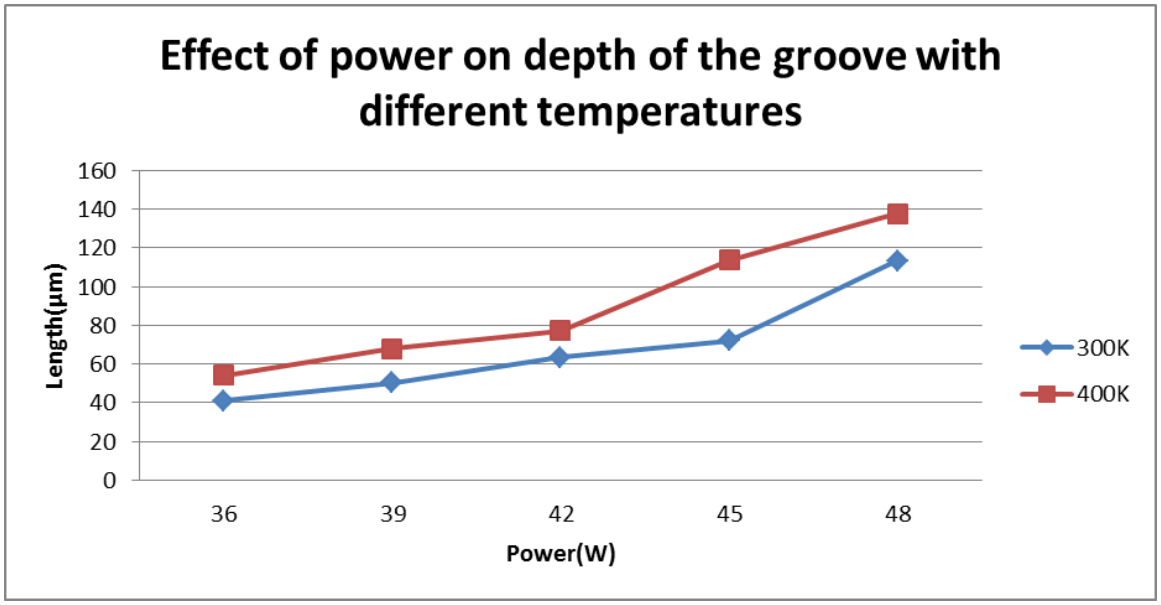

Figure 8.9 Effect of power on depth and width of the groove with different temperature

Another experiment was conducted to help us have better understanding of the temperature dependent property. Figure 8.9 shows that the relationship between power on depth and width of the groove with different temperature, in order to examine the laser absorption at different temperature when power is increased. According Figure 8.9, the higher temperature

induces deeper grooves. In addition, the sudden jump mentioned before happened between 45W and 48W at 300K; however, at 400K it happened earlier between 42W and 45W. This result means the higher temperature can make the stronger avalanche absorption happen at the lower power; it is another way to see the temperature dependent property.

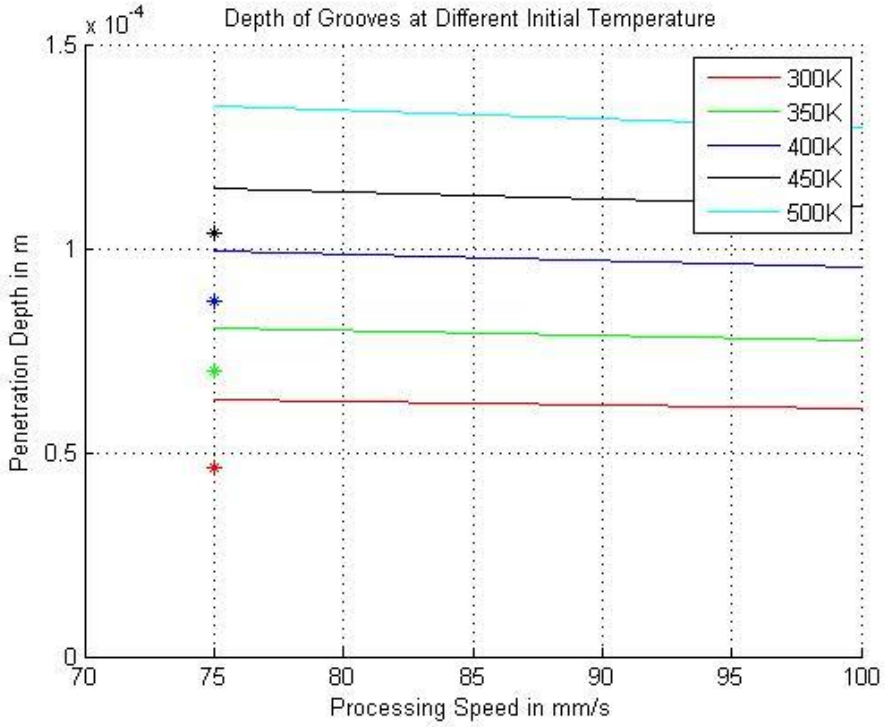

Figure 8.10Variation of penetration depth of solar cell at different initial temperature

Figure 8.10 shows the differences between the experimental results at different initial temperature and the prediction of the 2-D model. The star marks in different colors represent the experimental results, and the curves are the 2-D model. The results are predictable, and there is not much difference between the results and the model. The reason why the experimental results are smaller than 2-D model is because the model is assumed that 100% of the laser power is absorbed in the keyhole, but the absorption of silicon wafer is not 100%

at room temperature. When the initial temperature is higher, the absorption is closer to 100%, so that is why at higher temperature the experimental results are closer to the 2-D model.

8.4 Effect of different speeds on the groove

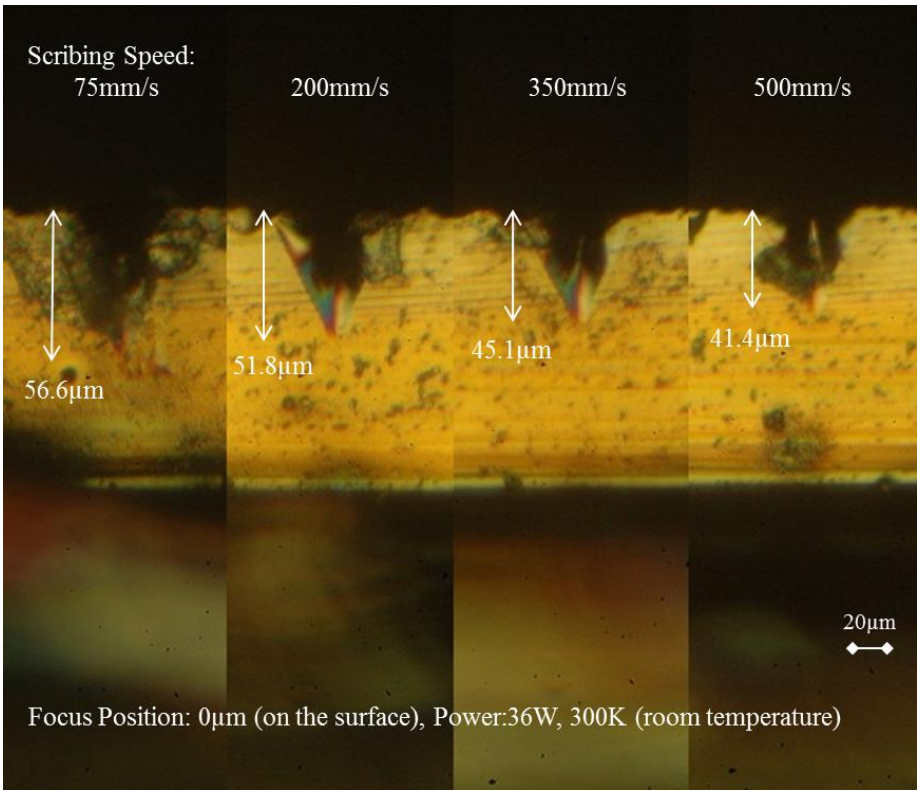

Figure 8.11 Depth of the grooves at different speed on the solar cell

Figure 8.14 shows the result of different speed on the welding depth. It can be observed that the depth of the groove becomes shallower as the scribing speed is increased. The result fits the 2-D welding model (Lankalapalli, Tu, *et al.*, 1996); the higher speed results in larger Péclet number, and the larger Péclet number is, the shallower the groove is. The contour of the grooves do not change much, still remaining the conical shape when the speed is higher.

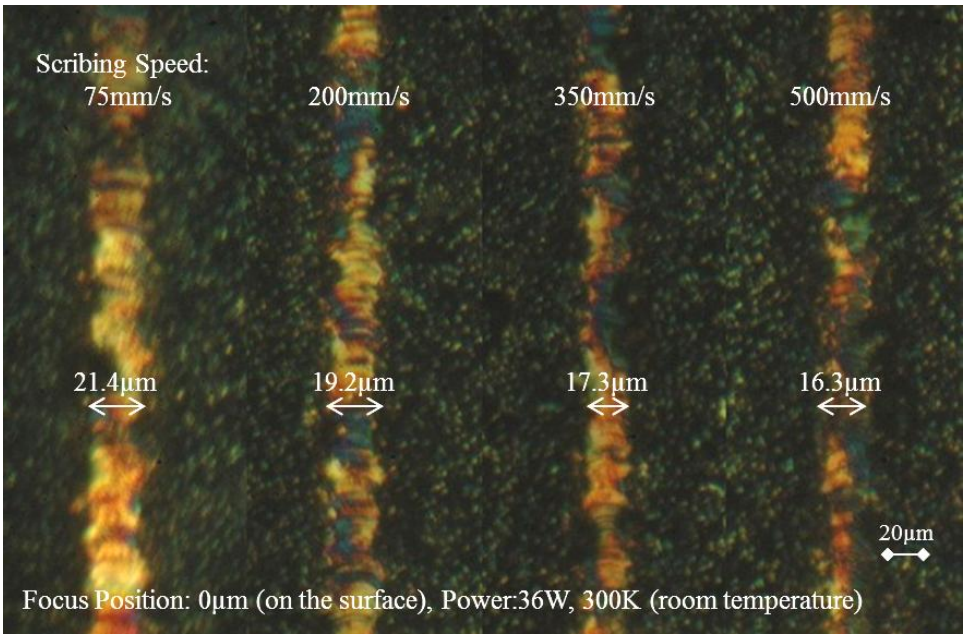

Figure 8.12 Width of the grooves at different speed on the solar cell

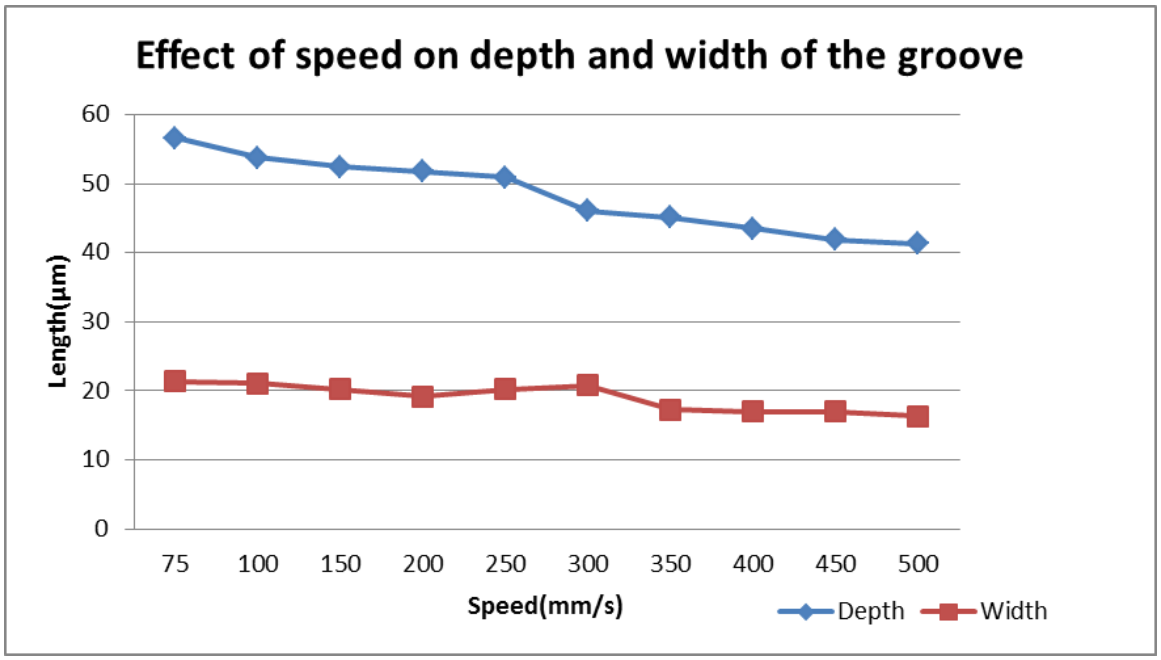

Figure 8.13 Width of the grooves at different speed on the solar cell

As we can see in Figure 8.15, there is no presence of crack on each groove at different speed, so the scribing speed is not the factor to cause this problem. Figure 8.16 shows the effect of focus position on the depth and width of the groove. The depth and the width both decrease when the scribing speed is higher, but the effect on the width is not distinct; the difference is only 5.1 μm between 75mm/s and 500mm/s. On the other hand, the effect on depth is much more obvious to be observed.

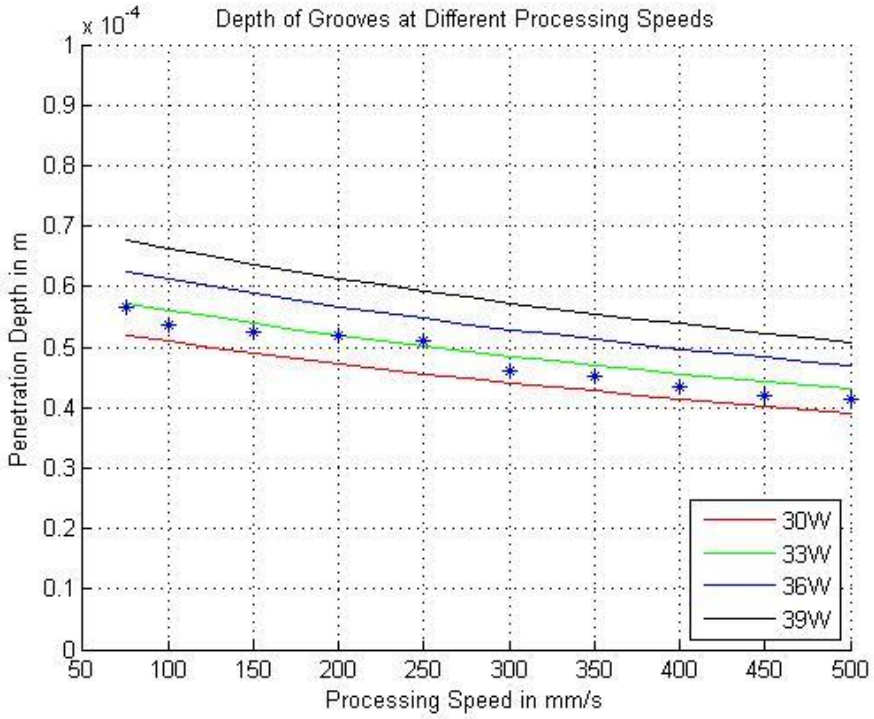

Figure 8.14 Variation of penetration depth of solar cell at different processing speeds

Figure 8.17 shows the differences between the experimental results cell at different processing speeds and the prediction of the 2-D model. The star marks in different colors represent the experimental results, and the curves represent the 2-D model. The 2-D model predicts the results very well; the results follow the trend of the curve. The reason why the experimental results are smaller than 2-D model is because the model is assumed that 100% of the laser power is absorbed in the keyhole, but the absorption of silicon wafer is not 100% at room temperature.

8.5 Systematic process design optimization

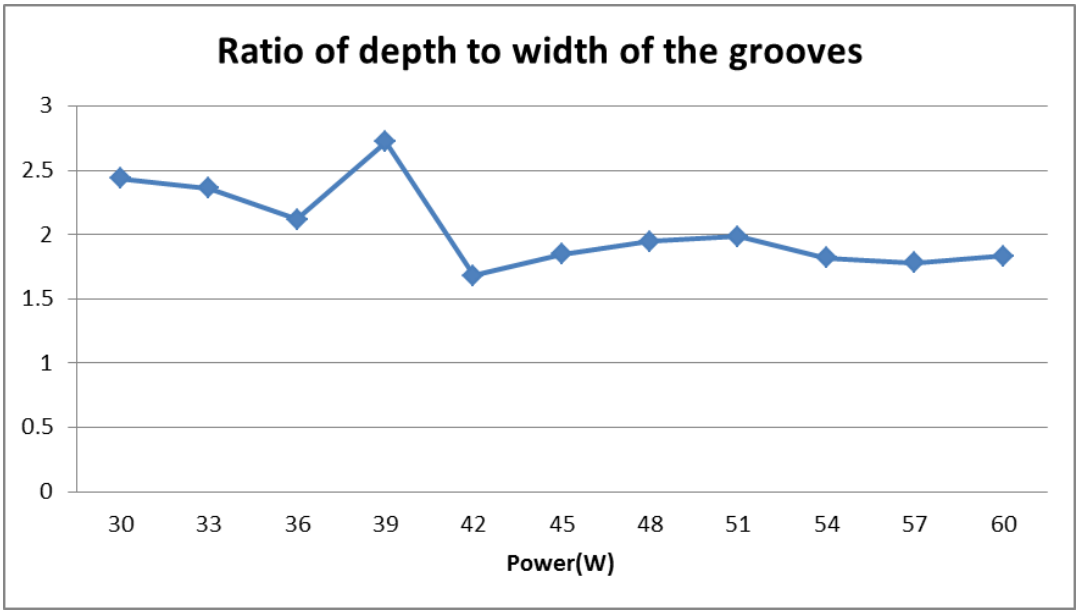

Figure 8.15 Ratio of depth and width of the groove at different powers

To optimize the edge isolation grooves to ensure the maximum area for sunlight absorption and better efficiency, those groove must be as deep and narrow as possible, which means the higher aspect ratio of the groove is preferred. Figure 8.18 is the result calculated from depth and width of the groove at different powers. We can learn from Figure 8.17 that at the lower power the ratio is higher, so using the lower power as possible can ensure not only crack-free groove but also better efficiency of solar cell.

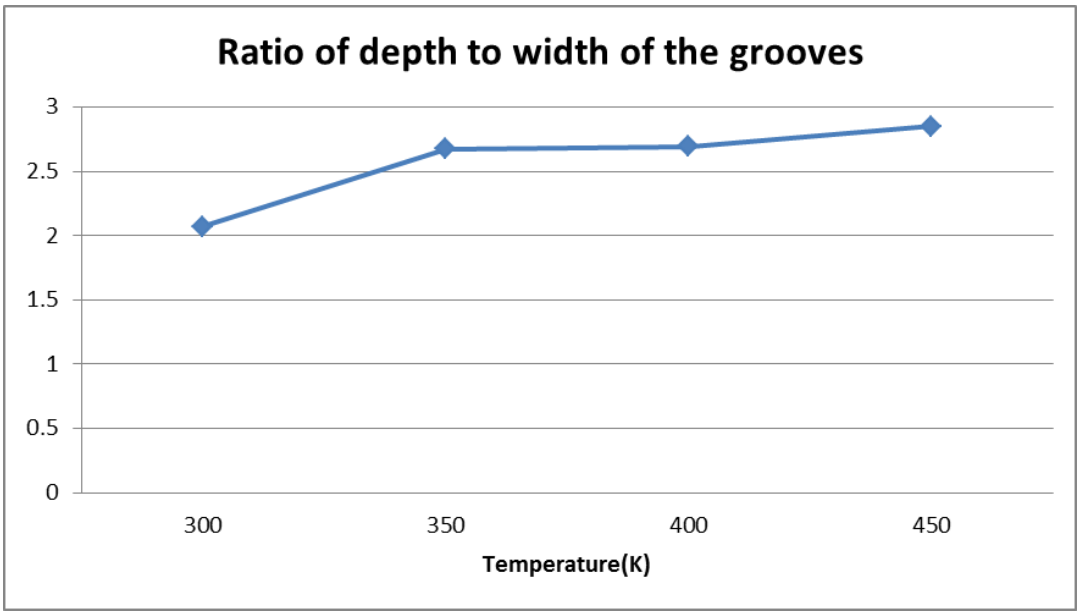

Figure 8.16 Ratio of depth and width of the groove at different temperature

To optimize the edge isolation grooves to ensure the maximum area for sunlight absorption and better efficiency, those groove must be as deep and narrow as possible, which means the higher aspect ratio of the groove is preferred. Figure 8.19 is the result calculated from depth and width of the groove at different temperature. We can learn from Figure 8.19 that at the higher temperature the ratio is higher, so increasing the temperature of solar cell as high as possible can ensure better aspect ratio grooves, resulting in better efficiency of solar cell.

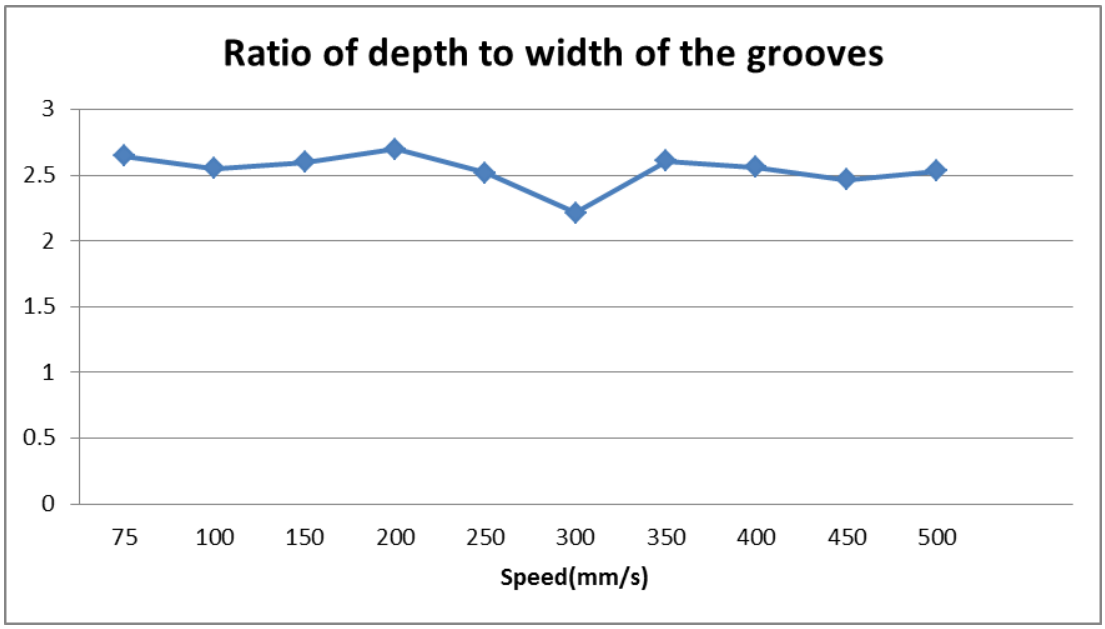

Figure 8.17 Ratio of depth and width of the groove at different processing speed

To optimize the edge isolation grooves to ensure the maximum area for sunlight absorption and better efficiency, those groove must be as deep and narrow as possible, which means the higher aspect ratio of the groove is preferred. Figure 8.19 is the result calculated from depth and width of the groove at different processing speed. The ratio of the scribing speed does not change very much from low to high. As far as the processing time is concerned, the faster speed is preferable.

9 SUMMARY AND CONCLUSIONS

The objectives of this research are to study temperature dependent optical properties of crystalline silicon and to investigate the feasibility of temperature manipulation for crack-free laser isolation. The absorption of laser energy by silicon is strongly influenced by its temperature; the absorption coefficient μ increases at elevated temperatures due to temperature dependent optical properties of crystalline silicon. Taking advantage of temperature dependent optical properties of silicon, one can compensate for the lower absorption of laser energy with 1064-nm wavelength.

Based on our study, it is true that if a preheating heat source is given, the laser absorption of silicon increases so that a deeper and wilder groove can be created. A 2-D welding model can predict the penetration depth inside the silicon. By using this model, the results of different process parameters such as scribing speed, incident power, and initial temperature can be estimated and predicted. The deep focus by pulsed laser explains the condition for void formation inside the material.

Experimental procedures were carried out to examine the theoretical analysis. The effects of the different process parameters on the geometry of grooves are studied. Systematic process design optimization for edge isolation is developed in order to ensure the maximum area for sunlight absorption and better efficiency. High preheating temperature field is preferable to make silicon have better laser absorption. Laser at lower power can avoid cracks and ensure higher aspect ratio groove. Focus position at 60 μm deep into the substrate has the highest aspect ratio groove, and focus position deeper that 160 μm deep into the substrate should be avoided for crack-free edge isolation. Last, the processing speed has little effect on the groove, but high speed is preferable as far as the time efficiency is concerned.

10 FUTURE WORK

In this research, it is mainly focused on studying study temperature dependent optical properties of crystalline silicon. Taking advantage of the properties, the temperature manipulation of crystalline silicon can be achieved for the edge isolation processing. However, the temperature dependent optical properties still can be explored further. If we can find ways to control the avalanche spot location and the propagation direction of the thermal shock, it becomes feasible to manipulate the nano-crystalline structure of doped silicon at specific locations not only for edge isolation but also for cutting purpose.

In the future, it is worth solving for a temperature inversion problem to determine the requirements of laser power, speed, and focusing position in order to achieve a prescribed temperature field. With the temperature field induced by laser heating more accurately predicted and the favorable conditions of the avalanche absorption determined, we can now define a desirable temperature field for manipulating nano-crystalline structure. To induce this desired temperature field, we seek to solve an inversion problem to determine the necessary laser control such that the actual temperature field can approach the desired temperature field.

REFERENCES

Hauser, A., G. Hahn, M. Spiegel, and H. Feist. 2001. “Comparison of Different Techniques for edge Isolation” Proceedings of the 17th European Photovoltaic Solar Energy Conference.

"Thermal Shock - Wikipedia." Wikipedia. http://en.wikipedia.org/wiki/Thermal_shock (accessed May 12, 2009).

Dirk-Holger Neuhaus and Adolf Munzer, Industrial silicon wafer Solar Cells, Advances in OptoElectronics Volume 2007

Colville, Finlay and Dunsky,Corey, 2008 “Lasers Support Emerging Solar Industry Needs” Photonics Spectra April 1, 44-47

German Foundation for Solar Energy . Photovoltaics: Solar Electricity and Solar Cells in Theory and Practice. 22 Jun. 2009. 22 Jun. 2009 <http://solarserver.de/wissen/photovoltaik-e.html>.

Hamammu, I. M., and K. Ibrahim, 2002. "Solar Cell Edge Shunt Isolation : A Simplified Approach." IEEE International Conference On Semiconductor Electronics Proceedings (2002): 230-232.

Komp, Richard J. Practical Photovoltaics: Electricity from Solar Cells. Walnut Creek, CA: Alta Mira Press, 2002

National Instruments. Part II – Photovoltaic Cell I-V Characterization Theory and LabVIEW Analysis Code. 25 Feb. 2009. 14 Apr. 2009 <http://http://zone.ni.com/devzone/cda/tut/p/id/7230>

RENA, "Wet Chemical Edge Isolation for Solar Cells." PhotoVoltaics 29.2 (2007): 8-9

Scott, Aldous. How Solar Cells Work. 1 Apr. 2000. 25 June 2008 <http://www.howstuffworks.com/solar-cell.htm>

Stay, Keith. "Getting the Most Out of PV Cells." PhotoVoltaics 29.2 (2007): 15-16

Paleocrassas, A.,2005,"Feasibility investigation of laser welding aluminum alloy 7075-T6 through the use of a 300W, single-mode ytterbium fiber optic laser", NSCU electronic Thesis and Dissertaion.

Langenkamp, M., and O. Breitenstein. 2002. "Classification of shunting mechanisms in crystalline silicon solar cells." Solar energy materials and solar cells 72: 433-440

Compaan, Alvin D. 1995. "Laser processing for thin-film photovoltaics". Proceedings of SPIE Volume 2403: 224-231.

Ohmura Etsuji, Masayoshi Kumagai, Makoto Nakano, Kuno Koji, Fukumistu Kenshi, and Morita Hideki. 2008. "Analysis of processing mechanism in stealth dicing of ultra thin silicon wafer.". Journal of advanced mechanical design, systems and manufacturing. 2 (4): 540-549

Shanks, H. R., P. D. Maycock, P. H. Sidles, and G. C. Danielson, *Phys. Rev.* 130**,** 5 (1963) 1743-1748

K.N. Lankalapalli, J.F. Tu and M. Gartner , A model for estimating penetration depth of laser welding processes. Phys. D: Appl. Phys. 29 (1996), pp. 1831–1841

Marco, Mendes, and Park Jongkook. (2006, March). Wafer Processing with Short-pulsed UV DPSS Lasers. Advanced Packageing, *15*(3), 37-40

Arumughan, Jayaprasad, Thomas Pernau, Alexander Hauser, and Ihor Melnyk. 2005. "Simplified edge isolation of buried contact solar cells." Solar Energy Materials and Solar Cells 87 (1-4): 705-714

Kyeong Dohyeon, Muniappan Gunasekaran, Kyunghae Kim, Heejae Kim, Kwon Taeyoung, Moon Inyong, Kim Youngkuk, Han Kyumin and Yi Junsin, 2009. “Laser Edge Isolation for High-efficiency Crystalline Silicon Solar Cells”. Journal of the Korean Physical Society 55 (1): 124-128

Breitenstein, O., J. P. Rakotoniaina, M. H. Al Rifai, and M. Werner, 2004. “Shunt Types in Crystalline Silicon Solar Cells.” Progress in Photovoltaics : Reserch & Applications 12: 529-538.

Goetzberger, Adolf, Joachim Knobloch, and Bernhard Voss. 1998. “Crystalline Silicon Solar Cells.” New York City, NY: John Wiley & Sons, Inc..

Breitenstein O and Langenkamp M. 2002. “Classification of shunting mechanism in crystalline silicon solar cells.” Solar Energy Materials and Solar Cells 72 (1-4): 433-440

Markvart, Tom, and Luis Castaner. 2005. Solar Cells : Maretials, Manufactre and Operation. Oxford, UK: Elsevier Ltd..

Colville, Finley 2009. Laser processing enables high-efficiency silicon-cell concepts. Photovoltaics World, March 1, 44-49.

Barsch, N., K. Korber, A. Ostendorf, and K. H. Tonshoff. 2003. Ablation and cutting of planer silicon devices using femtosecond laser pulses.. Applied Physics A, Material Science & Processing 77: 237-242.

" How Solar Panels Work 2 : Sunlight to Electricity " – 2012 Solar Journey USA http://www.solarjourneyusa.com/bandgaps.php.

" How Solar Cells Work-Solar Cell Overview " – 2009 SPECMAT, lnc http://specmat.com/Overview%20of%20Solar%20Cells.html.

" How Products Are Made Volume 1- Solar Cell " – 2012 Advameg, lnc http:// www.madehow.com/Volume-1/Solar-Cell.html.

Bullock, Charles E. and Peter H. Grambs. *Solar Electricity: Making the Sun Work for You.* Monegon, Ltd., 1981.

Komp, Richard J. *Practical Photovoltaics.* Aatec Publications, 1984.

Making and Using Electricity from the Sun. Tab Books, 1979.

Crawford, Mark. "DOE's Born-Again Solar Energy Plan," *Science.* March 23, 1990, pp. 1403-1404.

Rajule, Nilesh Gunwantrao, 2009. “Crack-free Edge Isolation of the Si Solar Cell Using a Single Mode Fiber Laser. ”

Glassbrenner, C. J. and G. A. Slack, *Phys. Rev.* 134, 4A (1964) A1058-A1069.

APPENDIX

Appendix A. MATLAB program for Penetration Depth vs Initial Temperature

```
% Depth Penetration for Silicon
clear;
clc;
% Material Properties of Silicon
k = [149 119 98.9 87.5 76.2]; % Thermal conductivity in W/(m*K)
alpha = 15e-6;%80e-6;        % Thermal diffusivity in m^2/s
Tv = 2628;              % Vaporization temperature in K
% Model constants
C = [1.4359 11.461 -10.704 6.6166];
% Welding conditions
Pi = 36 ;         % Incident power in W
v = [.075];         % Welding speed in m/s
a0 = 30e-6;                    % Spot radius in m
T0 = [300 350 400 450 500];                    % Ambient temperature in K
PS=75:25:500;
%Pe0=0.0125:0.0001:0.7500;
for i = 1:18
   Pe0=0.075/2:0.025/2:0.5/2;
   %Pe0=0.0125:0.1475:0.75;
   %Pe0(i) = v(i) * a0 / (2 * alpha);
   for j = 1:5
      d(i,j) = (Pi / (k(j).* (Tv - T0(j)))) * (1 / (C(1) / 1 * Pe0(i)^(1-1) + C(2) / 2 * Pe0(i)^(2-1)
+ C(3) / 3 * Pe0(i)^(3-1) + C(4) / 4 * Pe0(i)^(4-1)));
end
end
spd = [75 80 85 90 95 100 130];
hold on;
plot(PS, d(:,1),'r');%, 'ro' 'ko' 'kx' 'k+' 'k.' 'k*'
```

```
plot(PS, d(:,2),'g');
plot(PS, d(:,3),'b');
plot(PS, d(:,4),'k');
plot(PS, d(:,5),'c');
plot(75, 46.4*10^-6,'r*',75, 70.1*10^-6,'g*',75, 87*10^-6,'b*',75, 103.7*10^-6,'k*');
h = legend('300K','350K','400K','450K','500K',5);
set(h,'Interpreter','none')
xlabel('Processing Speed in mm/s')
ylabel('Penetration Depth in m')
title('Prediction of Depth of Grooves at Different Initial Temperature')
axis([70 500 0 15e-5]);
grid
hold off;
```